DETECTING WEEDS FROM VHR SATELLITE AND UAV IMAGES USING PATTERN AND TEXTURE MEASURES.

MBURU LOISE WAMBUI
March, 2017

SUPERVISORS:
Ms. Dr.Ir. W. Bijker
Dr. V.A. Tolpekin

DETECTING WEEDS FROM VHR SATELLITE AND UAV IMAGES USING PATTERN AND TEXTURE MEASURES.

MBURU LOISE WAMBUI
Enschede, The Netherlands, March, 2017

Thesis submitted to the Faculty of Geo-Information Science and Earth Observation of the University of Twente in partial fulfilment of the requirements for the degree of Master of Science in Geo-information Science and Earth Observation.
Specialization: Geoinformatics

SUPERVISORS:
Ms. Dr.Ir. W. Bijker
Dr. V.A. Tolpekin

THESIS ASSESSMENT BOARD:
Prof. Dr. Ir. A. Stein (Chair)
Dr.Ir. T.A. Groen (External Examiner, University of Twente, ITC-NRS)

ABSTRACT

Agriculture is one of the main economic sectors of most countries in Africa. It is a source of food to the people, acts as a source of employment and also raw materials for some products. Most of farmers are mainly small-scale due to lack of adequate land for farming, manpower and finances to manage large-scale farming.

Weeds are a major threat to the crop yields. Most of the small-scale farmers do not tend to their land after planting of crops especially if they find another quick way of earning money. The crops are left to grow without being well taken care of hence, affecting crop yields.

This research looks at a methodology for automatic detection of the weeds in farm fields. The information could be of use to the government to ensure food security in the country, and also the agricultural extension officers who advise farmers on good farming practices.

The study was carried out using the LSD and SVM algorithms on the UAV and VHR satellite imagery between the months of August and November 2014 in Mali. This was carried out on two cotton fields selected from two clusters, filed 23 in cluster 3 and filed 18 in cluster 4. The UAV images were found to be useful in this research as compared to VHR satellite imagery which failed at crop row detection. GLCM texture features were also extracted to assess the effect of additional variables in detection.

The LSD algorithm was used in this study for the detection of the crop rows and the weeds were detected between the crop rows using the SVM algorithm. The LSD algorithm extracts straight lines from images and is combined with the Helmholtz principle method for the validation of the detected line segments. The Number of False Alarms (NFA) is defined where a threshold epsilon (ε) is set in such a way that for a line segment to be considered meaningful, the NFA of this line must be less than or equal to ε.

The validation of the detected crop rows was done using manually digitized row edges. The weeds were detected using the SVM (Linear and RBF) classifier where the cover percentage of the weeds class in the field was calculated. The results were compared to the field reference data provided by the STARS project in collaboration with ICRISAT Mali.

The results of crop row detection had a great impact on the subsequent detection of weeds. This is because the crop rows that were missed in LSD analysis were classified as weeds in the SMV analysis. The weed percentage cover obtained in the SVM classification for the two fields showed an increase in weeds every month. The LSD algorithm showed a potential for clear crop row detection in case of images with clear identifiable crop rows. The SVM classification proved to work well after masking of trees, which avoided confusion between weeds and trees.

ACKNOWLEDGEMENTS

TABLE OF CONTENTS

LIST OF FIGURES

LIST OF TABLES

LIST OF ABBREVIATIONS

ASM – Angular Second Moment
DN – Digital Number
EDLines – Edge Drawing Lines
ENVI – Environment for Visualizing Images
GHz - Gigahertz.
GLCM – Grey-Level Co-occurrence Matrix
GPS – Global Positioning System
HSIC - Hilbert – Schmidt Independence Criterion
HT – Hough Transform
ICRISAT – International Crops Research Institute for the Semi-Arid Tropics
LSD – Line Segment Detector
NA – Not Available
NFA – Number of False Alarms
NIR – Near Infra-Red
PC – Personal Computer
PCA - Principle of Components Analysis
RBF – Radial Basis Function
RS – Remote Sensing
STARS – Spurring a Transformation for Agriculture through Remote Sensing
SVM – Support Vector Machines
UAV – Unmanned Aerial Vehicles
VHR – Very High Resolution
WV-2 – WorldView-2

1. INTRODUCTION

1.1. Background

A weed is any plant that is considered obnoxious or unwanted especially when growing in a controlled setup such as farm fields, gardens, and so on. They hamper the production of crops through competition for soil nutrients, water, light and space (Ahmed et al., 2012). Weeds have a negative effect to crop production hence, there is need to look for effective and sustainable ways of controlling them in order to ensure consistent food supply globally (Sardana et al., 2016). In order to achieve proper weed management, it is important to come up with constructive ways to detect, map and monitor weeds accurately (Atkinson et al., 2014). The weeds are eliminated from farms using various methods including; manual removal by the farm labourers, mechanical removal especially for large-commercial farms and application of herbicides (Ahmed et al., 2012). In the sub-Saharan Africa, most of weeding is done through manual removal since agriculture is mostly small-scale.

The global climate is becoming rapidly unpredictable. Africa is one of the vulnerable continents in terms of changes in climate and especially more so in the northern part of the Sub-saharan Africa; making food security a major challenge (Vintrou et al., 2009). This makes it important to incorporate reliable scientific knowledge to maximize on agricultural production. Most of the small-scale farmers do not have access to the right information that could help them in decision making in terms of how to improve farming to ensure high crop production (Kuntagod et al., 2016)

The option to use satellite-based information for agricultural practices has been greatly considered by the research community and governmental bodies dealing with agricultural production (Vintrou et al., 2009). This makes monitoring of various agricultural practices possible, including weed detection.

1.2. Motivation and Problem Statement

Agriculture is one of the major economic growth and sustainability factor for most of the countries (FAO, 2015) especially in the developing countries. It is the source of the most important human need; food, provides raw materials for various products and is also a source of employment for the majority of the population. Most farmers in the Sub-Saharan Africa practice small-holder farming and are still using traditional methods of agriculture (Calzadilla et al., 2013). This is mainly due to lack of finances and knowledge of modern methods that can improve their crop yields. Technological advancement is evident in all areas of the economy and agriculture has not been left out. It is possible to achieve sustainable development in the field of agriculture by involving the participation of farmers in various agricultural technological developments (Otsuka & Kalirajan, 2008).

Control of weeds is a major challenge for most farmers, which often results in high production costs, low crop yields or increased environmental degradation due to poor weed control methods. To ensure high production at a low cost while at the same time ensuring good maintenance of the economies and the environment, more pressure has been put by creating an opportunity to engineers and scientists to work together and find a solution to weed management in crops (Pierce & Clay, 2007). Hence, there is need to look for weed management approaches that will have a positive effect to the cropping systems in the future.

Remote sensing is being widely used for weed control in large scale and commercial farming, for crop production management and monitoring. This is being done by differentiating weeds from crops through

automatic detection, although the approach is often affected by the spatial and temporal resolution of the images used. Automatic detection of weeds using low spatial resolution satellite images is not easy; especially during early phenological stages, making them inefficient for post emergence control of weeds (López-Granados et al., 2016). This leads to further need for technological advancement in the field, where use of higher spatial resolution satellite images, airborne as well as UAV images, are being considered. They also need to be of high temporal resolution in order to monitor the weeds at different crop stages.

Unmanned aerial vehicles (UAV) images and Very high resolution (VHR) satellite images have become of high importance in weed monitoring and mapping. Satellites that provide very high resolution images of up to less than 1m resolution are available and they allow detailed and exhaustive mapping (Rougier et al., 2016). On the other hand, images from UAVs are more advantageous compared to satellite images as they have a higher spatial resolution. They give more details on the ground, which makes detection of weeds more precise during all growth stages. They are also not affected by the cloud cover as flying is done at lower height than satellite and airborne imagery. They have limitations in that they are expensive especially when the area of study is too large, they are susceptible to wind conditions. It is also a cutting edge technology as most operators are still not able to deliver data that is of acceptable quality (Zongjian, 2008).

Merging of spectral and textural information helps in improving the classification of imagery (Bekkari et al., 2011; Ursani et al., 2012). This is so especially for very high spatial resolution imagery (Bergado, 2016), such as UAV and VHR imagery. Extraction of this information can be done using various approaches such as Grey-level co-occurrence matrix (GLCM) which is most widely used. It computes the occurrence of pairs of gray-level value pixels in an image. The maximum gray value of a pixel determines the size of the GLCM and the relationship between the pixels in GLCM is determined by varying lag and direction (Alemu, 2016)

There are a variety of weed species growing at the same time as the crops in a field. Most of them grow in the space between the crop rows and some have similar spectral characteristics as the crops in the farm hence making their detection much harder. It is important to develop a methodology that will facilitate accurate automatic detection of weeds in the crop fields.

This study proposes a methodology where weed patches growing between crop rows can be detected using Support vector machines (SVM), after discriminating the crop rows using Line segment detector (LSD) from UAV and VHR imagery. In most crop fields in Africa, crops are planted in rows, parallel to each other and the spaces between them are more or less the same. Depending on the type of crop in a particular field, the rows appear mostly to be of the same width although they may not be too straight. This is because they are done manually and not mechanized. The LSD algorithm locally detects straight lines where gray values of pixels on the image are changing abruptly from dark to light and vice versa (Grompone Von Gioi et al., 2012). SVM is a non-parametric classifier that allows separation of data into two or more classes. SVMs can perform linear classification where the classes are linearly separable and also non-linear classification where the classes are not linearly separable. (Bekkari et al., 2011).

This technology is mostly useful for the local and national government, non-governmental organizations who are interested in monitoring of the crop yields to ensure food security in the country. The information could also be used by agricultural extension officers who advice smallholder farmers on weeding as a field activity to ensure high crop yields.

1.3.   Research Identification

1.3.1.   Research Objective

The main objective of this research is to develop methodology for between-row weed detection in smallholder crop farms using pattern and textural measures from UAV and VHR satellite images using line segment detector algorithm and support vector machines classifier.

1.3.2.   Specific Objectives

The specific objectives of this research include:

1. To test the LSD and SVM, in weed detection on both UAV and VHR images.
    *   Use LSD algorithm in discrimination of crop rows using pattern measures
    *   Compare SVM linear SVM and non-linear SVM (RBF kernel) classifiers in detection of weed patches between crop rows
2. To assess how the different imagery with different spatial resolutions affect the detection results
3. To compare detection of crop rows and weeds using images with and without texture features
4. To assess how the extracted weeds, compare with the available reference data

1.3.3.   Research Questions

1. How efficient is the LSD algorithm in terms of accuracy in crop row detection in Mali?
2. How efficient is the LSD algorithm in terms of time in crop row detection in Mali?
3. How effective is weed detection after discrimination of crop rows?
4. What are the accuracies obtained after detection with Linear and non-linear SVM for the two different images?
5. Which imagery between the UAV and VHR satellite, gives high accuracy results for detection of weeds?
6. How does detection of both crop rows and weeds on images with texture features compare with detection without texture features?
7. Do the percentages of the automatically detected weeds coincide with the weed cover reported in the reference data?
8. What are the optimal parameters for the LSD and SVM algorithms for the different images?

1.4.   Innovation

The novelty of this research is to explore the integration of LSD algorithm and SVM classifier in automatic weed detection from UAV and VHR satellite imagery. Most of the similar studies have been carried out in Europe and United States where farming is mechanized. Weed detection has not been exploited in Africa where farming conditions are different and on small-scale. The study carried out in Mali by Njenga (2016) focused on spectral measures and therefore, integration of crop row and weed detection has not been carried out in this region. This would be an interesting study considering that the crop rows are not as straight as in Europe and United States since they are done manually. LSD has also been used for crop row detection in Nigeria (Alemu, 2016) where the fields are clearer and have higher density of the crops along the rows which is different from Mali. Hough transform has been widely used in the field of agriculture for purpose of weed detection but there are other segment detector algorithms like LSD that are yet to be further explored.

2. LITERATURE REVIEW

2.1. Methods of line segment detection

Line segment detection has become a useful operation and is used in several operations of image processing (Akinlar & Topal, 2011). There are various methods that have been used before for line segment detection; but an algorithm would be considered ideal if it is able to process any images despite their origin, size or orientation, giving results of high quality as expected. This means that there should be minimal false detections and not time consuming. It should also not require any parameter tuning but should work with the same default parameters for all type of images (Akinlar & Topal, 2011) . For all the existing line segment detection algorithms, there is none that can be considered as perfect for detection. This is mostly due to people having differences in the general understanding or inference of a certain scene (Grompone von Gioi, 2014).

There are various techniques that are used for detection of lines, curves and arcs. Hough transform is one of the most recognized tools in this area (Jianjun Ni et al., 2016). It was introduced in 1962 by (Hough, 1962). It is used to detect straight lines, circles and other curved structures if their parametric equation is known. The first users were Duda & Hart (1972) who used it to detect straight lines in an image. It uses a binary edge map as an input and unlike other methods, it produces long lines that have to be broken down to line segments using a post-processing step. There are different versions of HT, with each one trying to counter for different limitations of the standard one. They include Randomized Hough transform (Xu et al., 1990), Progressive Probabilistic Hough transform (Kiryati et al., 1991), Elliptical Gaussian Hough transform (Fernandes & Oliveira, 2008).

Another technique that computes an edge map and the generates line segments was proposed by Etemadi (1992). Chains of pixels are generated from the edge map and then the line segments are generated following these chains of pixels. The extraction of the line segments does not require any parameters but the extraction of the edge map requires parameters, decided upon by the user. Although the line segments and arcs produced are very well-localized, they are too many with many false positives (Akinlar & Topal, 2011). This is more so in images with noise, trees and clouds.

Other line segment detection tools are not based on binary edge maps as an input but use the normal images where the gradient orientation of the pixels is used. EDLines is one of such tools proposed by Akinlar & Topal (2011). It borrows heavily from Burns et al. (1986), Desolneux et al. (2000) and Grompone von Gioi et al. (2008). It is a fast method that produces robust and accurate line segments and also uses the Helmholtz principle in the line validation process. It is very similar to LSD, used in this study and discussed more in Section 2.2. The main difference is that it is much faster in terms of computation and has fewer false positives.

2.2. Line segment detector algorithm

Line segment detector is a machine learning algorithm that is fast and robust in detecting straight lines as line segments on images. It is an algorithm that has been developed based on the method of Burns et al. (1986) of extracting straight lines, combining with the Helmholtz principle validation method proposed by Desolneux et al. (2008).

The algorithm's input is a gray-level image which gives a list of detected line segments as an output. These lines are the part of the image where the gray levels of pixels are changing abruptly from dark to light and vice versa (Grompone Von Gioi et al., 2012). This is done by determining the level-line angle at every pixel after which a level-line field is generated. The level-line field is then divided into regions of pixels that are connected, which share the same level-line angle up to a certain tolerance τ, known as line support regions. Each of the formed line support regions could be considered as a line segment. The line segment must be affiliated with a corresponding rectangular object where the principal inertia axis of the line support region is considered as the main direction of this rectangle and the size is chosen in order to cover the full region.

In this rectangle, all pixels that have their level-line angle corresponding to its angle up to a certain tolerance τ are known as aligned points. The number of aligned points denoted as k, together with the number of pixels in the rectangle denoted as n, are counted and used for validation of whether the rectangle forms a detected line segment or not. Each rectangle must go through a validation process which is mainly based on two approaches; the *a contrario* approach and the Helmholtz principle (Grompone Von Gioi et al., 2012).
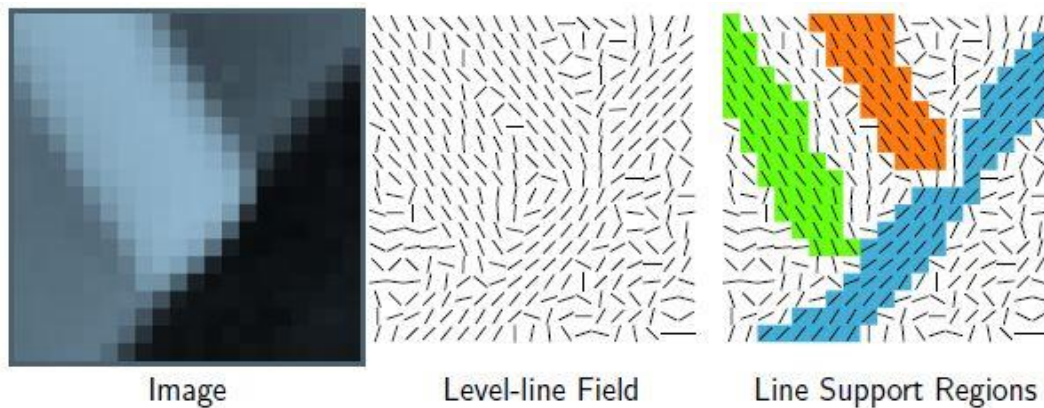
Figure 2.1: Processes in formation of line support regions. Source: Grompone Von Gioi et al. (2012)

2.2.1. The Helmholtz Principle

The Helmholtz principle was proposed by Desolneux et al. (2008). It works on a Gestalt theory also known as grouping, which is a law of visual perception (Desolneux et al., 2000). Points or objects that have some common characteristics like color consistency, parallelism, among others are grouped to form larger visual objects; which may further be grouped into other objects according to the characteristics that formed them in the first place. The Helmholtz principle validates the grouped objects by trying to depict when perception decides to group the objects according to a particular common characteristic (Desolneux et al., 2003). This way, it helps in controlling the number of false detections (Akinlar & Topal, 2011). The Helmholtz principle also indicates that an image with noise produces a poor detection (Grompone Von Gioi et al., 2012).

2.2.2. The *a Contrario* Approach

The *a contrario* approach is a statistical approach based on hypothesis testing where geometric meaningful events are detected (Desolneux, 2016). The probability of an observed geometric event under a noise model, also known as null hypothesis is computed and then the event is declared meaningful if the probability is small enough. In other words, the approach defines the null hypothesis (H_0) where the

desired structure is absent (Grompone Von Gioi et al., 2012). An event is only validated if the number of events that are expected to be as good as the observed ones are small in the *a contrario* model. This means that the structured events are considered as being uncommon in the *a contrario* model. The number of the aligned points is the most important in the case of line segments and therefore, a line segment in the *a contrario* model is deliberated as having an equivalent or more number of aligned points as the observed line segment.

2.3.   Number of False Alarms (NFA)

In order to ensure conclusive validation by the Helmholtz principle, false detections must be avoided. Desolneux in (Desolneux et al., 2000) defines the Number of False Alarms (NFA) of a line segment as: "Let A be a segment of length n with at least k points having their directions aligned with the direction of A in an image of size N x N pixels. Define NFA of A as:

$$NFA(n, k) = N^4 \cdot \sum_{i=k}^{n} \binom{n}{i} p^i (1-p)^{n-i} \qquad (2.1)$$

where N^4 represents the number of potential line segments in an N x N image because a line segment has two end points, and each end point can be located in any of the N^2 pixels of the image; thus, a total of N^4 x N^4 $= N^4$ line segments. The probability p used in the computation of the binomial tail represents the accuracy of the line direction". A threshold epsilon (ε) is set in such a way that for a line segment to be considered meaningful, the NFA of this line must be less or equal to ε, which is set at 1. The line segments whose NFA are more than ε are therefore rejected by the Helmholtz principle.

2.4.   Curved linear features

In man-made objects, some have straight edges while others have edges that are curved (Grompone von Gioi, 2014). Detection of curved edges using LSD gives a list of line segments forming the shape of the curved object with no information on their relative position; for instance, no information that two line segments follow one another along the same edge. Improving the detected line segments of the curved edge can be done using a chaining action that selects candidates that could form a continuous edge. This is done by finding a line segment after which the closest seed pixel to the end point of this line segment is selected and the process is repeated for the consecutive seed pixels allowing the chaining to be done manually following the curve (Grompone von Gioi, 2014). This helps in a better control of approximation of the curves by the line segments. The chaining of the edge pixels results in a rectangular polygon with the line segment candidates. The best approximation of the curves is determined by the fixed geometric thresholds which could be selected by use of the *a contrario* approach.

2.5.   Support Vector Machines

SVM is a non-parametric kernel based classification technique used in various application domains including image classification in remote sensing (RS). It is a supervised classification technique that aims at separation of two or more classes (Richards, 2013). SVMs are effective classifiers, considered currently among the most suitable techniques in RS classification. They are applied in classification of VHR images, multispectral images, hyperspectral data, aerial and UAV images among others to solve different types of classification problems (Bruzzone & Persello, 2010).

SVMs are considered suitable for image classification because, in order to carry out the classification, the classes are not required to be estimated by a statistical distribution but rather, the classification model is

defined by looking at the idea of margin maximization. This means that the classification is based on a margin-based/geometrical criterion rather than a purely statistical criterion. SVMs are also advantageous as they give results that are of high accuracy due to the structural risk minimization technique. They also have good generalization capabilities especially for classifications that are based on high dimensional feature space with few training samples. Another advantage is that they have a capability of separating non-linear classes by projecting the data onto a high dimensional feature space, then separating the classes using a simple linear function. Furthermore, in the learning phase, low effort is required in model selection with less control on parameters, hence reduction on computation time for the optimum parameter values selection.

2.5.1. Support Vector Machines classifiers

The SVM classifiers can be applied for classification of linearly separable classes and non-linearly separable classes. There are two types of SVMs, Linear SVM and Non-linear SVM. Linear SVM can further be divided into two where there is hard margin classification and soft margin classification.

With hard margin, the classification is applied for training sample classes that are linearly separable. Two parallel hyperplanes are selected that separate the two or more classes of data such that the distance between them is as large as possible. They also pass through the nearest training pixels from each class (Richards, 2013). This distance between the two hyperplanes is known as the margin while the maximum-margin hyperplane is the hyperplane that lies halfway between them. The points from the classes that fall along the two marginal hyperplanes are known as support vectors.
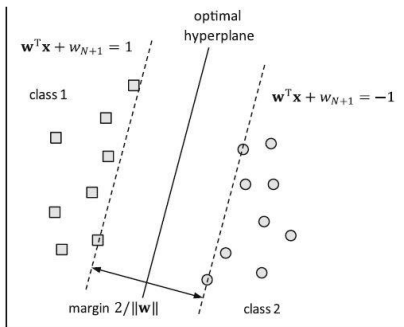
Figure 2.2: A separating hyperplane in the case of a linear separable classification problem. Source: Richards (2013).

In most cases, it is almost impossible to have pixels from the ground cover classes that are purely linearly separable. Therefore, soft margin is mainly applied in the case where two or more classes of data are not linearly separable or they overlap. This could be mainly due to noisy samples and outliers, in which case, a hard SVM cannot be used (Bruzzone & Persello, 2010). In this case, "slack variables" (ξ_i) are defined during the training step, which allow easy handling of consequences brought about by misclassification due to the overlapping of these training samples (Richards, 2013).

.
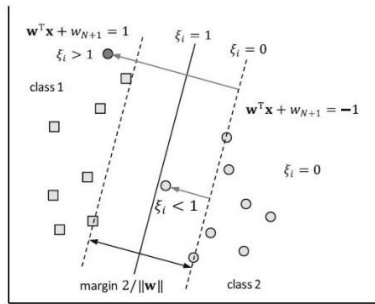
Figure 2.3: A separating hyperplane in the case of a non-linear separable classification problem. Source: Richards (2013).

An improvement soft margin SVM algorithm could also be done where non-linear classifiers are created by applying a kernel trick to the maximum margin hyperplanes. A non-linear kernel function replaces every dot product or scalar which allows fitting the maximum margin hyperplane in to a transformed high dimensional feature space. This way, there is better separability of the transformed training samples (Bruzzone & Persello, 2010).
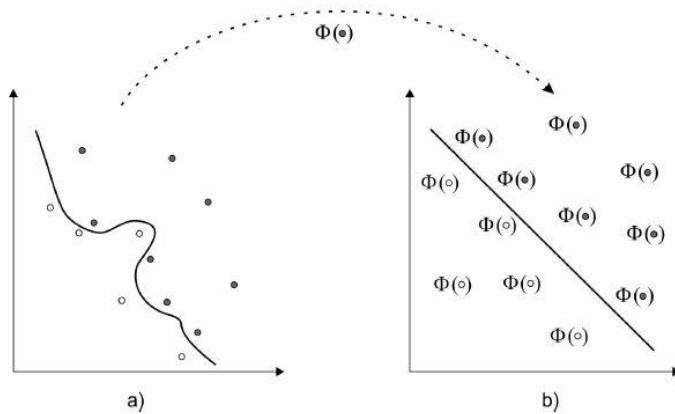
Figure 2.4: Example of a transformation of the training samples using a kernel function into a high dimension feature space. a) Input feature space; b) kernel induced high dimensional feature space. Source: Bruzzone & Persello (2010)

2.6. Texture measures

Texture of an image is given by a distinction in the spatial occurrence in the frequency and intensity of the gray level values of every pixel in an image (Malegori et al., 2016). It plays an important role during image analysis as a measure of identifying various objects of interest in images of different kinds, such as Aerial images, UAV images and Satellite images. (Haralick et al., 1973). Calculation of texture features through a co-occurrence matrix of the gray levels is the technique mostly used for surface analysis in images. This is where the number of rows and columns of an image is equal to the number of gray levels in the image, known as gray level co-occurrence matrix (GLCM) (Malegori et al., 2016).

The technique of GLCM was introduced by Haralick et al. (1973), whose importance is to ensure contribution of many variables to represent the intricacy of a phenomenon; which is met through the Principle of Components analysis (PCA). Through PCA, the observed variability is well explained. The phenomenon is described by two or more orthogonal dimensions arranged according to their significance

in the variance explanation (Malegori et al., 2016). There are 14 GLCM textural features, some of which are highly correlated and hence, no need to use all of them in image analysis (Haralick et al., 1973).

3.   STUDY AREA AND DATA DESCRIPTION

3.1.   Study area

This study is carried out in Sougoumba, Sikasso Region in Mali. The area is located in the southern part of the country, at location coordinates 12°10'20"N 5°11'20"W. The southern region of the country is where most of agricultural production is practiced. The main crops grown in Mali include corn, millet, sorghum, paddy rice, peanuts, cotton, vegetables, with corn, millet and rice being the basic crops. Cotton is the main crop produced for exportation and is the country's largest foreign earner in the agricultural sector (Nations Encyclopedia, 2015).

For most of the crops grown in this region, the growing season is mainly between the months of June and November; with May being the month when crop fields are prepared for planting.
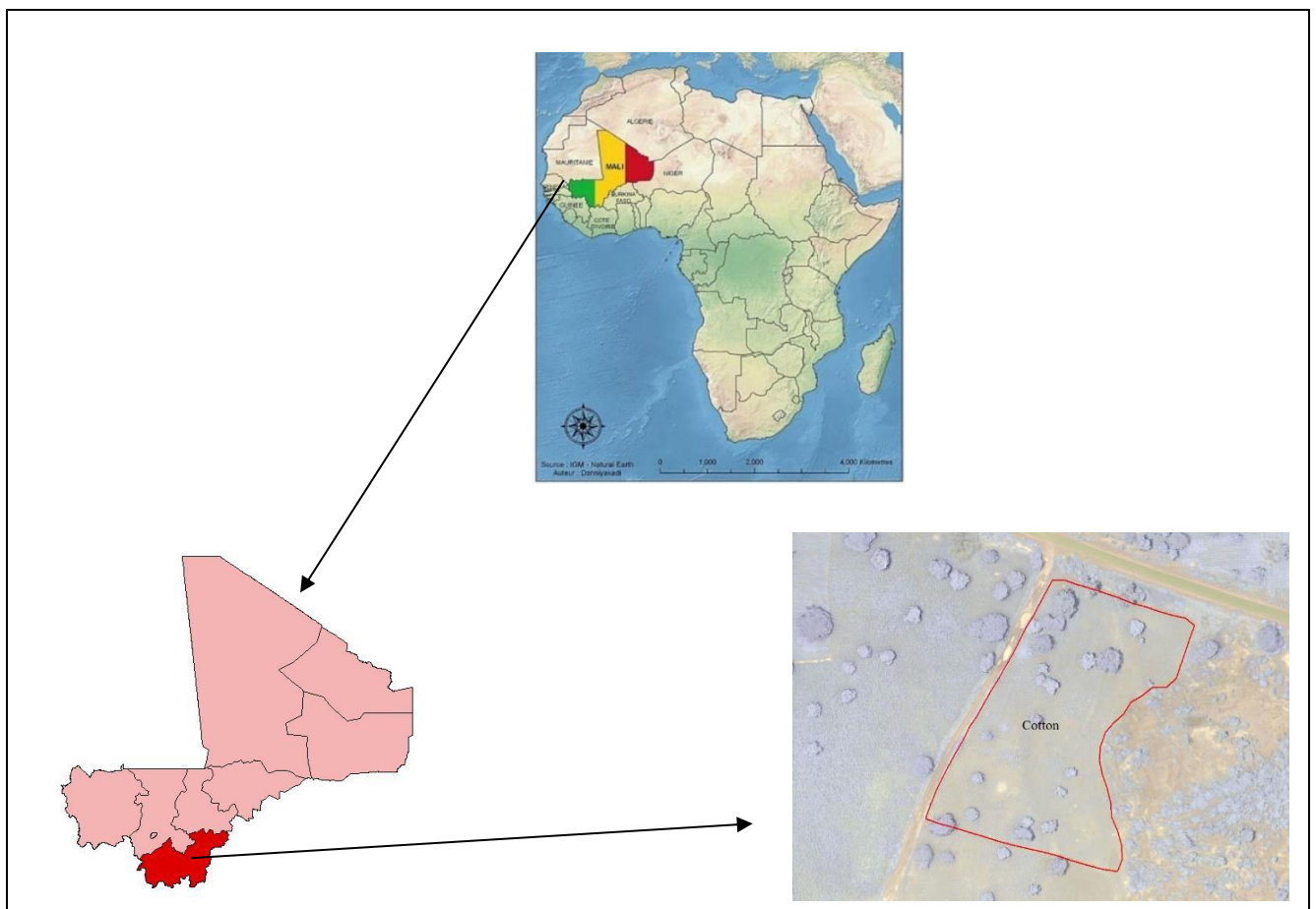
Figure 3.1: Study area. Top image shows the location of the Mali on the map of Africa, lower left map is the whole of Mali with Sikasso region highlighted in red and lower right is the 2014 UAV image showing one of the cotton fields used in the study.

3.2. Data description

3.2.1. Very high resolution satellite images

The satellite images available for the study in this area include WorldView-2, QuickBird and GeoEye-1 satellite images for the year 2014. These are available between the months of May and November 2014. The resolution of the panchromatic bands is between 0.41 and 0.61 meters while for the multispectral bands is between 1.65 and 2.44 meters. The images used in the study are selected from all the three sensors during the mid-growing season. The criteria for selection is looking at the images free of clouds especially on the fields being analysed and also when the crops are already established in the fields. The selected images include:

- WorldView-2 – 29th July 2014
- GeoEye-1 – 25th September 2014
- Quickbird – 26th August 2014

The World View 2 satellite was launched on 8th October 2009. It has a resolution of 0.46 m and 2 m for the panchromatic band and the multispectral bands respectively. The panchromatic band has a spectral range between 450 nm and 800 nm. On the other hand, it has eight multispectral bands with different spectral ranges which include; Coastal (400 – 450 nm), Blue (450 – 510 nm), Green (510 – 580 nm), Yellow (585 – 625 nm), Red (630 – 690 nm), Red Edge (705 – 745 nm), Near Infrared (NIR) 1 (770 – 895 nm) Near Infrared (NIR) 2 (860 – 1040 nm). It has a swath width of 16.4 km and a revisit time of 1.1 days.

The GeoEye-1 satellite was launched on 6th September 2008. It has a resolution of 0.41 m and 1.65 m for the panchromatic band and the multispectral bands respectively. The panchromatic band has a spectral range between 450 nm and 800 nm. The 4 multispectral bands include; Blue (450 – 510 nm), Green (510 – 580 nm), Red (655 – 690 nm) and Near Infrared (780 – 920 nm). It has a swath width of 15.3 km at nadir with a revisit time of 2.6 days.

The QuickBird satellite was launched on 18th October 2001. It has a resolution of 0.61 m and 2.44 m for the panchromatic band and the multispectral bands respectively. The panchromatic band has a spectral range between 405 nm and 1053 nm. The 4 multispectral bands include; Blue (430 – 545 nm), Green (466 – 620 nm), Red (590 – 710 nm) and Near Infra-Red (715 – 918 nm). It has a swath width of 16.8 km at nadir with a revisit time of 5.9 days.

3.2.2. Unmanned Aerial Vehicle (UAV) Images

The UAV images used in this study were provided by the STARS project in collaboration with ICRISAT Mali. They include images captured between August and December 2014, having a fine resolution of 10 cm and three bands; Red, Green and Near Infra-Red. The images were captured using an eBee platform with a NIR camera. This was done in clusters as shown in Figure 3.3, as it would not have been possible to capture one image covering the whole study area. The study area was divided into seven clusters, where images were captured every two weeks per cluster within the five months. Figure 3.2 shows the timeline for the image acquisition for each cluster. UAV images in clusters 3 and 4 are used in this study, analysing one image per month. This is because the two clusters have images taken almost same dates and the capturing is also consistent between late August and November when the crops are well established in the fields up to the harvesting time.
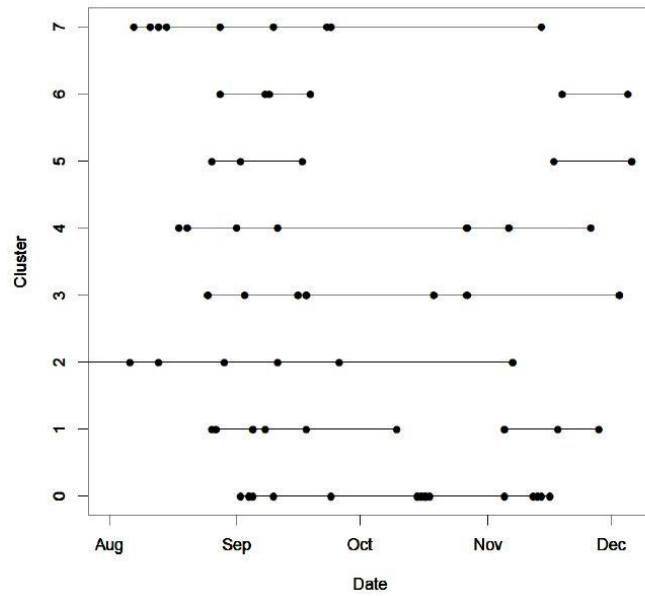
Figure 3.2: UAV acquisition timeline per cluster. Cluster 3 and 4 are selected for this study. Source: STARS & ICRISAT (2015)
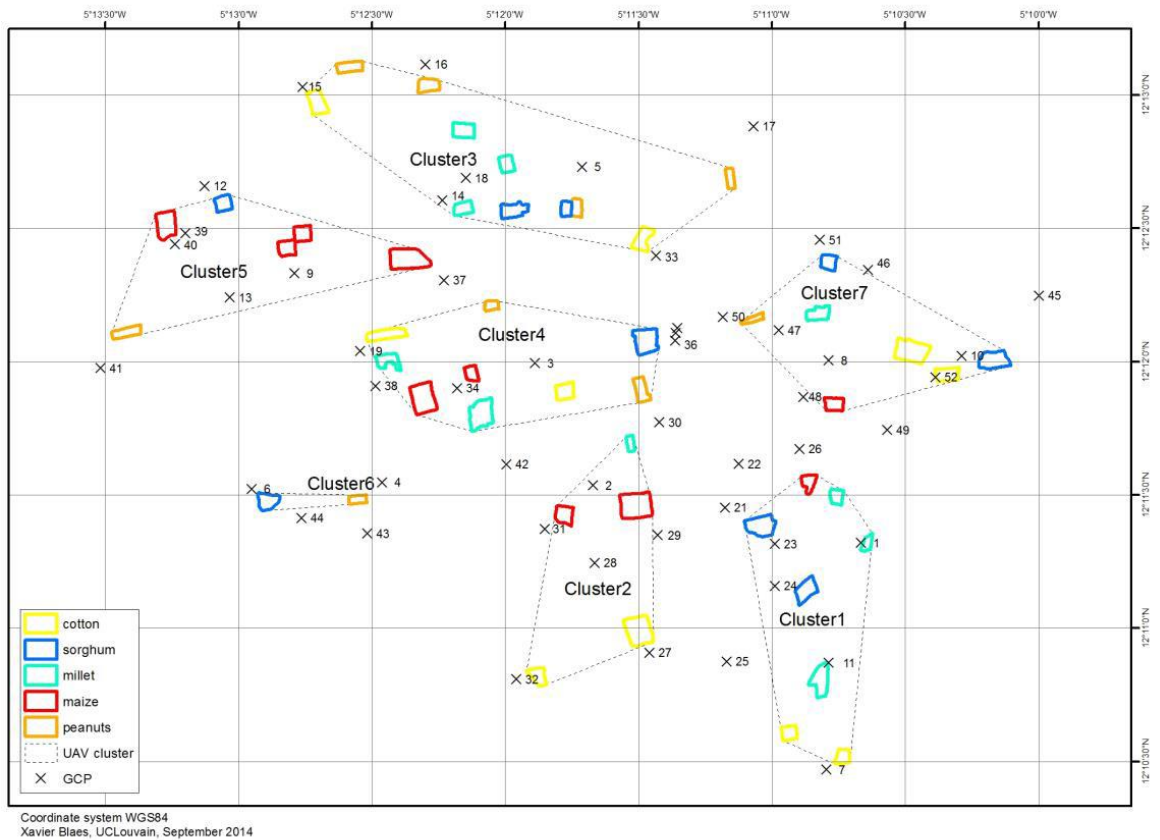
Figure 3.3: Map showing the location of the 7 clusters. Each cluster has field boundaries with colour coded crop type. Clusters 3 and 4 are selected for this study. Source: STARS & ICRISAT (2015)

3.2.3. Reference dataset

Field data collected in the fields during the 2014 growing season was provided by the STARS project in collaboration with ICRISAT Mali. This data includes shapefile of 48 field boundaries with different crop types as shown in Figure 3.3. They were recorded using a GPS Trimble JUNO with no any differential correction. The accuracy position of the field boundaries is between 5 and 10 meters. The attributes of the field boundaries include names of the field owners, the field number, the crop type grown and the eBee cluster number that the field belongs to.

After assessing the UAV images, two cotton fields, one in cluster 3 and another in cluster 4, are used for the analysis of crop rows and weeds in this study. The fields selected are field number 23 in cluster 3 as shown in Figure 3.4 and field number 18 in cluster 4 as shown in Figure 3.5. The reason for using cotton fields in this study is because the cotton fields were observed to have clearer and identifiable crop rows compared to all other crop types within the study area. The sowing date for field number 23 was 23rd June 2014 and only one weeding carried out throughout the entire season, done on 10th July 2014. The sowing date for field 18 was 10th June 2014 and no weeding done throughout the entire growing season.

Information on the various activities carried out in the fields within the entire growing season was also recorded. This data was collected at 2 m x 2 m quadrat level and then aggregated to 15 m x 15 m plots. The information included; the soil type, dates of fertilizer application, ground cover, canopy cover, dates of weeding, yield in metric tons, weed biomass, crop biomass, presence or absence of weeds, weed cover per quadrat in grams. The weed cover information for the two fields was measured between 15th August and 17th September 2014. This was recorded as a range of 0%; <10%, 10 – 50% and >50%.

In this study, the information on percentage range of weeds cover is used as the reference data in weed detection. The field photos captured at different point in the quadrats were also used for verification of presence of weeds in the fields. The reference data used in crop row detection is manually delineated from the UAV images. This is done by manually digitizing the edges of the crop rows using the ArcGIS software.
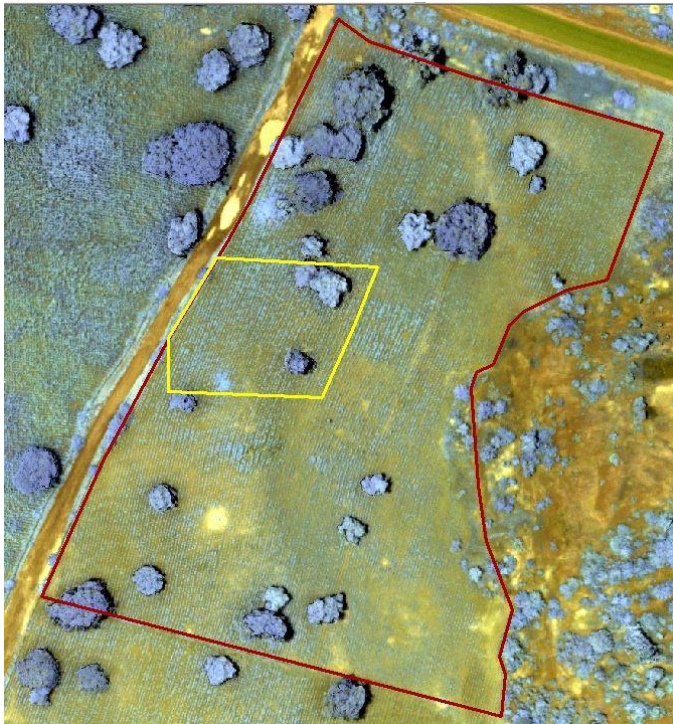
Figure 3.4: UAV image of field 23 in cluster 3 captured on 25th August 2014. The outer boundary is the entire extent of the field, the yellow inner boundary is a subset used in the analysis (band combination – R-Red, G-Green, B-NIR)
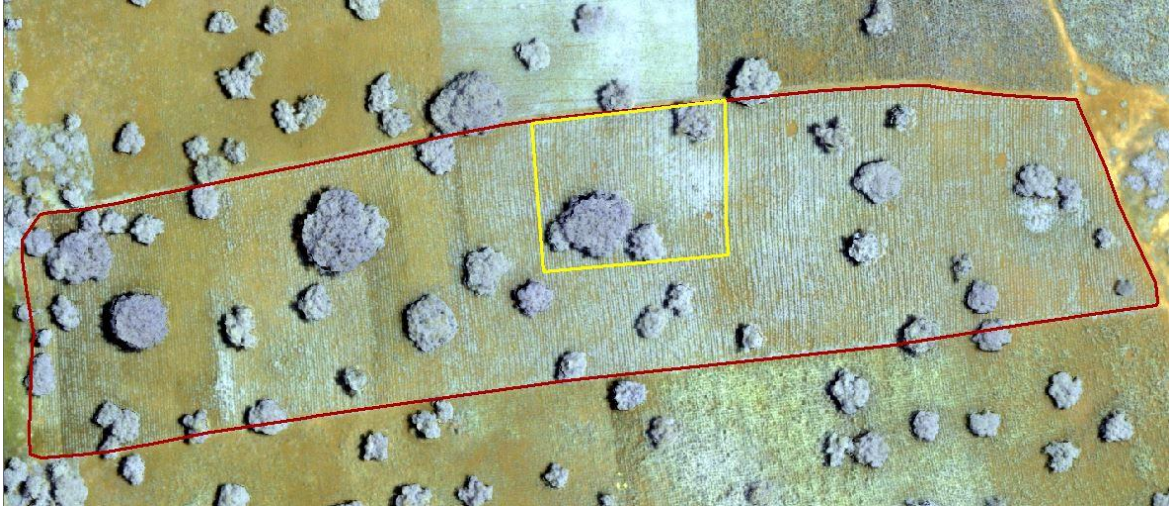
Figure 3.5: UAV image of field 18 in cluster 4 captured on 20th August 2014. The outer boundary is the entire extent of the field, the yellow inner boundary is a subset used in the analysis (band combination – R-Red, G-Green, B-NIR).

4. METHODOLOGY

4.1. GLCM feature extraction

In an image, the GLCM features can be extracted in up to eight directions of the nearest neibours to the pixel of interest. This is not necessary as a GLCM is usually considered to be symmetric, where pixels directly opposite one another from the pixel of interest are the same (Clausi & Jernigan, 1998), and have the same spatial distance to that pixel. Hence, only four directions, (0°, 45°, 90° and 135°) are important when extracting the texture features. The texture features in this study are extracted using the ENVI software. For each pixel being analysed, the features were extracted in the four directions and at lag distances d = 1, 2 and 3 for window size 3 x 3 and d = 1 for window size 5 x 5.

As discussed in Section 2.7, there are 14 types of GLCM features that can be extracted but not all of them are useful as some are highly correlated hence, would result in redundancy. The statistics of texture features used in this study are eight, (mean, contrast, angular second moment, variance, dissimilarity, correlation, homogeneity and entropy) with notations $p(i,j)$ and N_g , where $p(i,j)$ is the normalized gray level in the cell $(i,j)^{th}$ of the spatial dependence matrix while N_g is the number of clear gray levels in the quantized image (Haralick et al., 1973).

The mean GLCM feature is calculated by:

$$\text{Mean} = \sum_{i=1}^{N_g-1} \sum_{j=1}^{N_g-1} ip(i,j) \qquad (4.1)$$

The contrast texture feature determines the contrast or local intensity between a pixel and its neighbouring pixels all over an image. Pixels with similar DN values give low contrast resulting to poor distinction between objects in an image. The equation for contrast intensity is:

$$\text{Contrast} = \sum_{n=0}^{N_g-1} n^2 \left\{ \sum_{i=1}^{N_g} \sum_{j=1}^{N_g} p(i,j) \right\}, \qquad |i-j| = n \qquad (4.2)$$

Angular second moment (ASM) is a measure of textural uniformity or homogeneity in an image. Pixels that are uniform in gray level distribution result in maximum energy of texture. ASM is given by:

$$\text{ASM} = \sum_{i=0}^{N_g-1} \sum_{j=0}^{N_g-1} \{p(i,j)\}^2 \qquad (4.3)$$

The variance is a measure of roughness in an image. It is calculated by:

$$\text{Variance} = \sum_{i=0}^{N_g-1} \sum_{j=0}^{N_g-1} (i-\mu)^2 \, p(i,j) \qquad (4.4)$$

Dissimilarity feature is calculated as follows:

$$\text{Dissimilarity} = \sum_{i=0}^{N_g-1} \sum_{j=0}^{N_g-1} p(i,j)|i-j| \qquad (4.5)$$

Correlation feature shows how a reference pixel has a spatial linear dependency to its neighbouring pixels in an image. It considers the mean and standard deviation of the row and column in the matrix. It is calculated by:

$$\text{Correlation} = \sum_{i=0}^{N_g-1} \sum_{j=0}^{N_g-1} \frac{\{i \cdot j\} \cdot p(i,j) - \{\mu_x \cdot \mu_y\}}{\{\sigma_x \cdot \sigma_y\}} \qquad (4.6)$$

where μ_x, μ_y, σ_x, σ_x are the mean and standard deviation of p_x and p_y respectively.

Homogeneity is the closeness of the gray level values in the spatial distribution in an image. It is calculated by:

$$\text{Homogeneity} = \sum_{i=0}^{N_g-1} \sum_{j=0}^{N_g-1} \frac{p(i,j)}{1 + |i-j|} \qquad (4.7)$$

Entropy measures the uniformity of the gray level distribution in an image. Homogeneous scenes in an image have high entropy while inhomogeneous scenes have low entropy. It is calculated by:

$$\text{Entropy} = -\sum_{i=0}^{N_g-1} \sum_{j=0}^{N_g-1} p(i,j) \log(p(i,j)) \qquad (4.8)$$

4.2. Crop row detection

The crop row detection is carried out using the LSD algorithm. This algorithm extends the work of Burns et al. (1986) of line segment detection and integrates it with the line validation method due to the Helmholtz principle by Desolneux et al. (2008). Different internal parameters require to be estimated in order to get a set of the most optimal ones that give the most accurate line segments.

4.2.1. Image scaling and gradient magnitude

During the LSD analysis, the original image requires to be downscaled to a coarser spatial resolution. This is to ensure that the image is brought to a scale where the most of the crop rows are detectable including the ones that appear smallest on the image (Sidiropoulou et al., 2015). This is done by using a scale factor less than 1 ($S < 1$). The image $f(x,y)$ is filtered using the derivative of Gaussian, G with $\sigma = \frac{0.8}{S}$. The image is filtered in the horizontal direction (g_x) and vertical direction (g_y). Image gradient is the directional change in intensity which is used for extraction of information from images. (Grompone von Gioi, 2014; Akinlar & Topal, 2011). Figure 4.1 show an example of image gradient for horizontal and vertical directions. The pixel gradient (g_x) and (g_y) in the x and y directions is calculated as:

$$g_x = \frac{\partial(G * f)}{\partial x} = \frac{\partial G}{\partial x} * f \qquad (4.9)$$

$$g_y = \frac{\partial(G * f)}{\partial y} = \frac{\partial G}{\partial y} * f$$

(4.10)

where $*$ is the convolution operation which is associative.

The gradient magnitude Z is calculated as:

$$Z(x, y) = \sqrt{g_x(x,y)^2 + g_y(x,y)^2}$$

(4.11)

The gradient direction or the level-line angle of the pixel (x, y) is calculated as:

$$\phi(x, y) = \arctan\left(\frac{g_x(x,y)}{-g_y(x,y)}\right)$$

(4.12)

The level line angles are responsible for change in direction of the edge or the angle of dark to light transition. Transitions from dark to light are not the same as light to dark because of the 180° angle difference in the corresponding gradient. Therefore, line segments with different transitions are oriented but the order of their start and end points are different since the algorithm encodes the darker side of the edge.
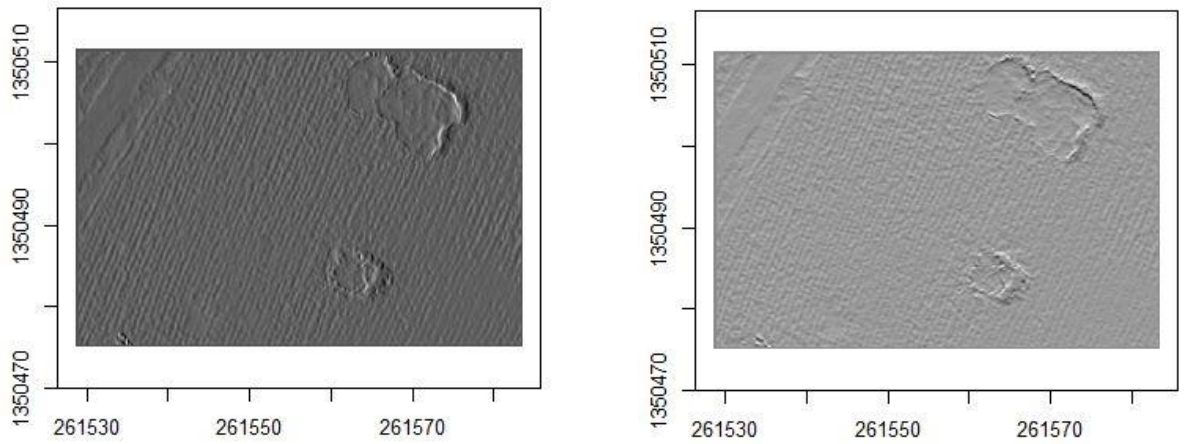
Figure 4.1: Example of image gradient in different directions. Left image is gradient in the horizontal direction (g_x) while the right image is gradient in the vertical direction (g_y).

4.2.2. Angular tolerance parameter (τ)

This is the parameter that joins the aligned pixels into a line support region. As discussed in Section 2.2, each line support region is a candidate for a line segment. By "aligned", it means that a line segment with 2 points A and B have the same direction; meaning that the points are aligned with a precision of $\frac{1}{n}$ if angle A and angle B are within $\frac{\pi}{n}$ degrees of one another.

Using a neighbourhood of 16 pixels or $\tau = 45°$ results in regions expanding too far from the edge while a neighbourhood of 4 pixels or $\tau = 11.25°$ is limiting with the region obtained being too small as seen in Figure 4.3. Therefore, 2 points are always assumed to be aligned if their angles are within $\frac{\pi}{8}$ or 22.5° of each other. The actual value of τ is not the most important but the order of magnitude. It is therefore set to obtain precision p which is the likelihood that a pixel has an explicit orientation in the *a contrario* model. The precision p is set at $\frac{\tau}{180°}$. Different values of τ are tested in this study to evaluate their effect on the LSD results.
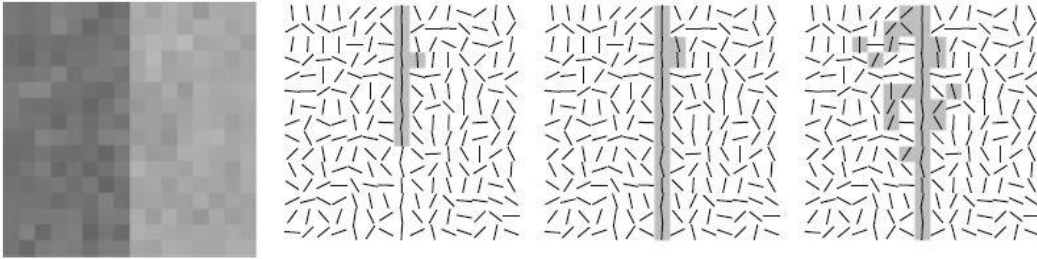
Figure 4.2: Example of line support regions obtained at varying τ. From left to right: Image; $\tau = 11.25°$; $\tau = 22.25°$ and $\tau = 45°$. Source: Grompone Von Gioi et al. (2012)

4.2.3. Gradient threshold and ordering

The order in which pixels are analysed in LSD has an effect on the output result. Pixels of high gradient magnitude result in edges with more contrast. Since the central pixels in an edge has a higher gradient magnitude, the algorithm starts looking for line segments at these pixels (Grompone von Gioi, 2014). Once the gradient computation is done, all pixels that have gradient values with less than a certain threshold are ignored for chaining of segments. This allows omission of pixels that do not contain edgels.

In this study, the minimum gradient magnitude threshold for region growing is performed using quantile-based thresholding, which is a way of binarizing high gradient magnitudes (Teutsch, 2014). The threshold ω_q is selected depending on the way the gray values of pixels are distributed in an image. In the gradient magnitude image, all of its gray values are assembled together in a histogram. The quantile value q divides the histogram into two gray value parts that is, lighter and darker gray value parts. The q value should be between 0 and 1. If it is set at a very low value, it leads to features on the image that have poor contrast being undetectable. On the other hand, if set too high, it results in detections that are merged.

4.2.4. Region growing

In this step, the line support regions are formed. The algorithm gets the ordered pixels (the seed) to form a line support region. It also tests the neighbouring pixels that are within the region (R); adding to it the ones whose level-line angle is the same as the region angle θ_R up to a tolerance τ. The initial θ_R is usually set to the level-line angle of the seed pixel and as new neighbouring pixels are added to R, the θ_R value is updated by:

$$\theta_R = \arctan\left(\frac{\sum_j \sin \theta_j}{\sum_j \cos \theta_j}\right) \tag{4.13}$$

where index j runs over the pixels inside R while θ_j is the level-line angle. The process is done iteratively as shown in Figure 4.3 until no more neighbouring pixels within R are added to it. Figure 4.4 shows an example of an image with ordered pixels that form line support regions.
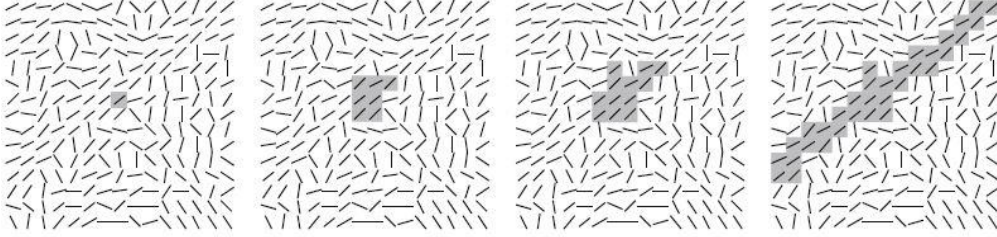
Figure 4.3: Iterative formation of the regions shown by the pixels highlighted in gray. Sorce: Grompone von Gioi (2014)
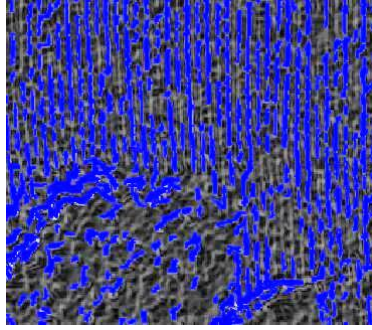
Figure 4.4: Example of a gray scale image with ordered pixels (in blue) that form line support regions

4.2.5. Rectangular approximation

At this point, the line support regions are evaluated in order to determine whether they are meaningful or not. As indicated earlier in Section 2.2, a line segment must be affiliated with a corresponding rectangular event which must be found for the line support regions to be evaluated. The region (R) of pixels is considered as a solid object with every pixel's gradient magnitude used as the mass of that point. The middle of the mass of R is then chosen as the middle of the rectangle, with the main direction of the rectangle being set to the first inertia axis of R. The length and the width of R are then set to the smallest values that make the rectangle to make the full line support region as seen in Figure 4.5. To get the centre of the rectangle (c_x, c_y), the following formula is used.

$$C_x = \left(\frac{\sum_{j \epsilon R} g(j) . x(j)}{\sum_{j \epsilon R} g(j)} \right) \qquad (4.14)$$

$$C_y = \left(\frac{\sum_{j \epsilon R} g(j) . y(j)}{\sum_{j \epsilon R} g(j)} \right) \qquad (4.15)$$

where $g(j)$ is the gradient magnitude of pixel j in R. Index j runs over all the pixels in R. The rectangle's direction is set to the eigenvector angle, which is connected to the smallest eigenvalue of the matrix:

$$M = \begin{pmatrix} m_{xx} & m_{xy} \\ m_{xy} & m_{yy} \end{pmatrix} \tag{4.16}$$

where

$$m_{xx} = \frac{\sum_{j\epsilon R} g(j) \cdot (x(j) - c_x)^2}{\sum_{j\epsilon R} g(j)} \tag{4.17}$$

$$m_{yy} = \frac{\sum_{j\epsilon R} g(j) \cdot \left(y(j) - c_y\right)^2}{\sum_{j\epsilon R} g(j)} \tag{4.18}$$

$$m_{xy} = \frac{\sum_{j\epsilon R} g(j) \cdot (x(j) - c_x) \cdot \left(y(j) - c_y\right)}{\sum_{j\epsilon R} g(j)} \tag{4.19}$$
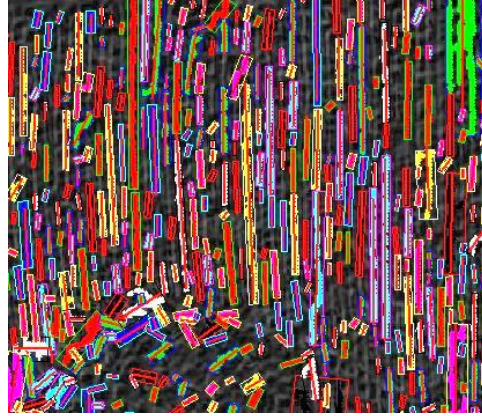
Figure 4.5: Rectangles covering the line support regions with line segments at the center of the rectangle.

4.2.6. NFA computation

This is the line validation step which is based on the Helmholtz principle. It is an *a contrario* approach where the objects are detected as outliers in the background model (Akinlar & Topal, 2011). It depends on the precision p, set initially to $\frac{\tau}{\pi}$, with τ being the angular tolerance used in region growing. In a rectangle, the total number of pixels are represented by n while the number of p-aligned points represented by k. The number of false alarms related to the rectangle is given by:

$$NFA(r) = (NM)^{5/2} \gamma \cdot B(n, k, p) \tag{4.20}$$

where N and M are the number of rows and columns of the image after scaling, while γ is the number of p that are tested. $B(n, k, p)$ is the binomial distribution's tail; given by:

$$B(n, k, p) = \sum_{j=k}^{n} \binom{n}{j} p^j (1 - p)^{n-j} \tag{4.21}$$

In all the rectangles evaluated and allocated a precision p, the numbers of k and n are calculated, after which their NFA values are computed as follows:

$$NFA(r) = (NM)^{5/2} \gamma \cdot \sum_{j=k}^{n} \binom{n}{j} p^j (1 - p)^{n-j} \tag{4.22}$$

As indicated in Section 2.3, for a rectangle to be considered having valid detections, the value of NFA has to be less or equal to the epsilon (ε) which is usually set as 1. In this analysis, different values of ε are tested to see the effect on the result.

4.3. Parameter tuning

The various internal parameters in the LSD algorithm were tuned in order to get the set that produced the most optimal results in terms of the correct detection of the edges of the crop rows. The parameters tuned included the minimum gradient magnitude threshold for region growing (ω), scale (S), angle tolerance (τ), detection threshold – epsilon (ε) and the threshold of detection for the smallest area in pixels. This was done by tuning each parameter at a time while keeping the rest fixed. They were tuned in order of their occurrence in the algorithm. The scale parameter was the first to be tuned while the rest were kept at their default values. This was then followed by the gradient magnitude threshold for region growing, angular tolerance, epsilon and finally the threshold of detection for the smallest area in pixels. The UAV image used for the tuning process was the subset of cotton field 23 in cluster 3 captured on 25th August 2014. The Satellite image used for this process was WorldView-2 captured on 29th July 2014.

4.4. Approximating the undetected edges of the crop rows

The detection of crop rows on the UAV image was resulting in only one side of the row being detected. This could be due to the quality of the image and also the position of the drone during capturing of the images. The side of the crop row that formed a shadow is the only side that was automatically detected by the LSD algorithm. There was therefore a need to approximate the other side of the row in order to get the two edges. This would help in facilitating better detection of weeds in the next step of the study.

The orientation angle of the detected lines was calculated in order to check the orientation dominance of the detected lines that represent crop rows. This is important to ensure that the detected rows have the same orientation as the actual crop rows in the field. The orientation was calculated by getting the angle theta of each detected line as follows:

$$\theta = \arctan\left(\frac{\Delta y}{\Delta x}\right) \tag{4.23}$$

where Δy and Δx are changes in y and x for the detected line segments respectively.

This was simplified to only the first two quadrants of the circle (0° - 180°). A histogram was then plotted in order to show how the orientation of the detected lines appears and the range with the highest peak on the histogram was considered as the lines with the same orientation as the actual crop rows in the field. The ones outside this range, which did not represent the crop rows were then discarded.

A manual check of the width of the rows was done by measuring the width of the majority of rows in the field. The width ranged between 0.4 – 0.55 m. Therefore, an approximate width of 0.5 m was chosen and used to approximate the other side of the row. This was done in ArcGIS by copying parallel of the lines at an offset of 0.5 m either to the right or the left of the lines depending on which side of the row required to be approximated. This is because images of different dates produced lines detected on different sides of the crop rows.

4.5.   Accuracy assessment and validation

The accuracy of the detected crop rows was assessed by cross-checking the detected lines with the manually digitized rows. The manually digitized crop rows were captured using the ArcGIS software as discussed in Section 3.2.3.

A part of the process in Section 4.3 for getting the orientation dominance was repeated for both the detected lines and the manually digitized rows. After getting the angle of orientation for both sets of lines, rose diagrams were plotted for graphical presentation, showing the comparison between the detected lines and the manually digitized ones.

4.6.   Weed detection

The main importance of this study is the detection and analysis of the weeds in the fields in Mali. After the detection of the crop rows, the next step was to detect the weeds using the SVM algorithm. This was carried out on the UAV images as detection of crop rows in the satellite images had failed.

The process required to detect the weeds that are between the crop rows. In order to ensure that only the pixels with vegetation that represent anything else except for the crop rows are analysed for weed detection, the detected crop rows were first masked out of the image, leaving the values of pixels of the crop rows as NA values. Linear and RBF SVM were then applied on the masked images for weed detection. This was done on images with and without texture features.

4.6.1.   Selection of training, test and validation data sets

Labelled data known as the training set and test set are selected that are used to train the SVM classifier and test it for accuracy assessment. The training data set should be selected in such a way that the polygons represent all classes of interest and if possible all classes represented in the subset of image to be classified (Richards, 2013). The training data set is randomly selected with each polygon labelled as the class that it should represent during the training of the SVM.

The test data set is a sample of randomly selected pixels that are used to assess the accuracy of the SVM classification. Their labels are checked against the actual ground samples or the training data. The test set is similar to the training set and therefore, in most cases, the two data sets are randomly selected as one, labelled to represent the different classes and then a subset is used as training pixels and another subset used as the test pixels.

4.6.2. Parameter tuning – Linear SVM

The Linear SVM used for classification in this study is the soft margin SVM for overlapping classes where slack variables are introduced as discussed in Section 2.6.2. During the training of the classifier, the number of erroneous training samples are minimized while at the same time maximizing the margin. The parameter that requires tuning is the *"regularization parameter"* (C), which is a positive weight that helps in regulating the relative importance of the margin against the misclassification error (Richards, 2013). This parameter is always selected at each classification of different data as it varies according to the data input. It should be selected in an accurate model selection phase as a precise value is very important for the accuracy of the classification result. It should also neither be too small nor too large as a very small value of C leads to erroneous results leading to underfitting of the classifier while the latter may lead to overfitting of the classifier. This leads to poor generalization of the classifier. The algorithm estimates the best C by setting a search grid where values are selected then used to train the SVM one by one until the best value is arrived at. This value is then used to produce the classification result.

4.6.3. Parameter tuning – RBF SVM

RBF SVM kernel was also applied on the UAV images for weeds analysis in this study. The parameters required to be tuned include gamma (γ) and the regularization parameter (C) (Richards, 2013). γ is the width parameter in the RBF kernel and determines the effect of a single training sample. Low values of γ mean the kernel is very wide and high values mean that the kernel is very narrow. The two parameters are interdependent and therefore one cannot be estimated without the other.

Different data sets give different values for the best C and γ. Therefore, the two have to be estimated for each classification process. These can vary over a wide range, especially the C parameter thus, the need for an efficient search strategy. The algorithm uses a grid search strategy that is set to select an initial range of values of pairs of the two parameters. This is followed by training of the SVM using set of pairs selected in turns after which the best value for C and γ are selected.

4.6.4. Feature selection

During the analysis of weeds using images with the texture features, feature selection is done to reduce the number of the features used for the analysis since not all features give optimal results. This is important as it helps to; reduce computational burden of the algorithm, reduced storage memory, avoid confusion of the algorithm due to redundant and irrelevant features and finally avoid errors due to reduced generalization capability (Song et al., 2012).

For data X and Y, there is a set of features (A), where each element in A represents one dimension of the data. A subset $B \subseteq A$ is selected with the relevant information in X being maintained. If the data is computed while being restricted to dimensions in B and the relevance of information is measured by $Q(B)$, formulation of feature selection is then as follows:

$$B_0 = \underset{B \subseteq A}{\operatorname{argmax}} Q(B) \text{ subject to } |B| \leq (b) \tag{4.24}$$

where $|B|$ computes the number of elements of a set and b is the limit on the number of the selected features. For a feature selection criterion to be considered efficient, two conditions must be met. First, the measure $Q(B)$ should be able to detect the required functional dependence, whether linear or nonlinear, between the data and the training samples. Secondly $Q(B)$ should be applied with respect to the measure

being used. This ensures a high probability of the detected functional dependence being retained in the test samples.

The feature selection method used in this study is the Hilbert – Schmidt independence criterion (HSIC); which is a non-parametric measure of dependence. It does not only consider linear correlation between variables, but also all forms of dependence between the variables. It is an unbiased empirical estimate that guarantees a good uniform convergence. It also meets the two conditions that are required for $Q(B)$ (Song et al., 2012).

4.6.5. Masking of trees

The noise in the UAV images affect their quality, making all types of vegetation on images to appear as having similar reflectance values. Some of the pixels that represent tree features have same DN values as the pixels representing weeds. This is also observed in the crops and therefore, most of the vegetation in the UAV images appear to have similar pixel values. The errors brought about by the confusion between weeds and crops was minimized by the detection of the crop rows and masking them before SVM classification for weed detection.

There is need for precise detection of weeds and this would only be possible by trying to avoid as many errors as possible. For this reason, the trees within the fields where the classification was carried out were masked from the image; in order to avoid confusion between the trees and weeds classes. This was done manually by digitizing the trees using the ArcGIS software and then masking them out the same way the crop rows were masked. In case of classification of a large area, this task would require to be automated. In this study, the task was not automated because it was not part of this study and is only done to ensure higher accuracy. The area analysed is also not large and the manual digitization of the trees was very fast.

4.7. Accuracy assessment and validation

After the SVM classification, the accuracy assessment and validation of the obtained results is carried out. One of the ways used in accuracy assessment is the use of the test samples as discussed in Section 4.6.1. The labels of the test data are checked against those of the training data used to train the classifier as the reference for classification. After this, the result is presented in form of a confusion matrix; where the training data classes are listed by column and the resulting classes as per the classification map are listed by row of the matrix. The overall accuracy is then calculated by getting the sum of the diagonal of the confusion matrix and dividing the value by the test samples.

The Kappa Coefficient is also a measure of accuracy assessment used in this study. It is derived from the confusion matrix and is assumed to be unbiased in terms of the chance agreement between the output result and the reference/training data.

The validation of the classification results obtained is carried out by use of the reference data provided by the STARS project in collaboration with ICRISAT Mali. After the classification, the area covered by the pixels classified as representing each class in the field is calculated. The area of the weeds class is then computed as a percentage, and compared to the reference data provided.

5. RESULTS

5.1. Crop row detection

5.1.1. Tuning of the scale parameter

As discussed in Section 4.2.1, the scale is important for downscaling of the image to ensure that most of the crop rows are detectable, even the smallest ones (Sidiropoulou et al., 2015). This parameter was tuned by trying out different values that included $S = 0.2$, $S = 0.5$, $S = 0.8$, $S = 1$, $S = 1.2$ and $S = 1.5$. At $S = 1$, this would be analysing the image at its original status of 100%. Figure 5.1 shows the results of tuning parameter S on the UAV imagery.

At both high and low extremes of the S values tuned, the results were unsuccessful. $S = 0.2$ produced few detections and most of the segments were incorrect. Most did not represent crop rows and others were on top and edges of trees. $S = 0.5$ produced the most number of line segments with most being incorrect. Some of the detected line segments were on top and edges of trees. $S = 1$ and $S = 0.8$ produced almost same results, with $S = 0.8$ producing a slightly higher number of line segments. Most of these segments were correctly detected as compared to the ones produced at lower S values. $S = 1.2$ and $S = 1.5$ produced most correct line segments although with a lot of missed detections. Most of the crop rows were not detected at these two values as compared to $S = 1$ and $S = 0.8$. Thus, $S = 0.8$ was considered as the most optimal value. The processing time of the algorithm in a PC with 2.40 GHz was 25.77 seconds.

Figure 5.1: Crop row detection at different scale (S) parameter values. Black segments are the reference lines, red segments are the detected lines

5.1.2.   Tuning of the magnitude quantile (q)

This parameter was tuned at different quantile q values of 0.25, 0.5, 0.7, 0.72, 0.74, 0.75, 0.76, 0.78 and 0.8. This was done in order to get the optimal value that ensures that features with poor contrast on the image are detectable and also there are no merged detections (Teutsch, 2014). The other parameters were kept default values of $S = 0.8$, $\tau = 22.5°$, minimum area in pixels = 10 and $\varepsilon = 1$. Figure 5.2 shows the results of UAV image at various magnitude quantile parameters tested. The reason for tuning many q values between 0.7 and 0.8 is because at $q = 0.7$ is where more stable results were realised.

It was observed that the lower the quantile value for thresholding tested, the poorer the detection. Improvement is observed at $q = 0.6$, which produced few lines that were long and continuous but mostly incorrect. The q values between 0.7 and 0.76 produced a higher number of detected lines but the higher the value, the more the missed detections. $q = 0.8$ produced lines correctly representing the rows but with a lot of missed detections. $q = 0.7$ was observed to produce more correct detections with less missed detections compared to other values and was therefore selected as the optimal value for gradient magnitude threshold. Figure 5.2 shows the results of some detections at different q values.
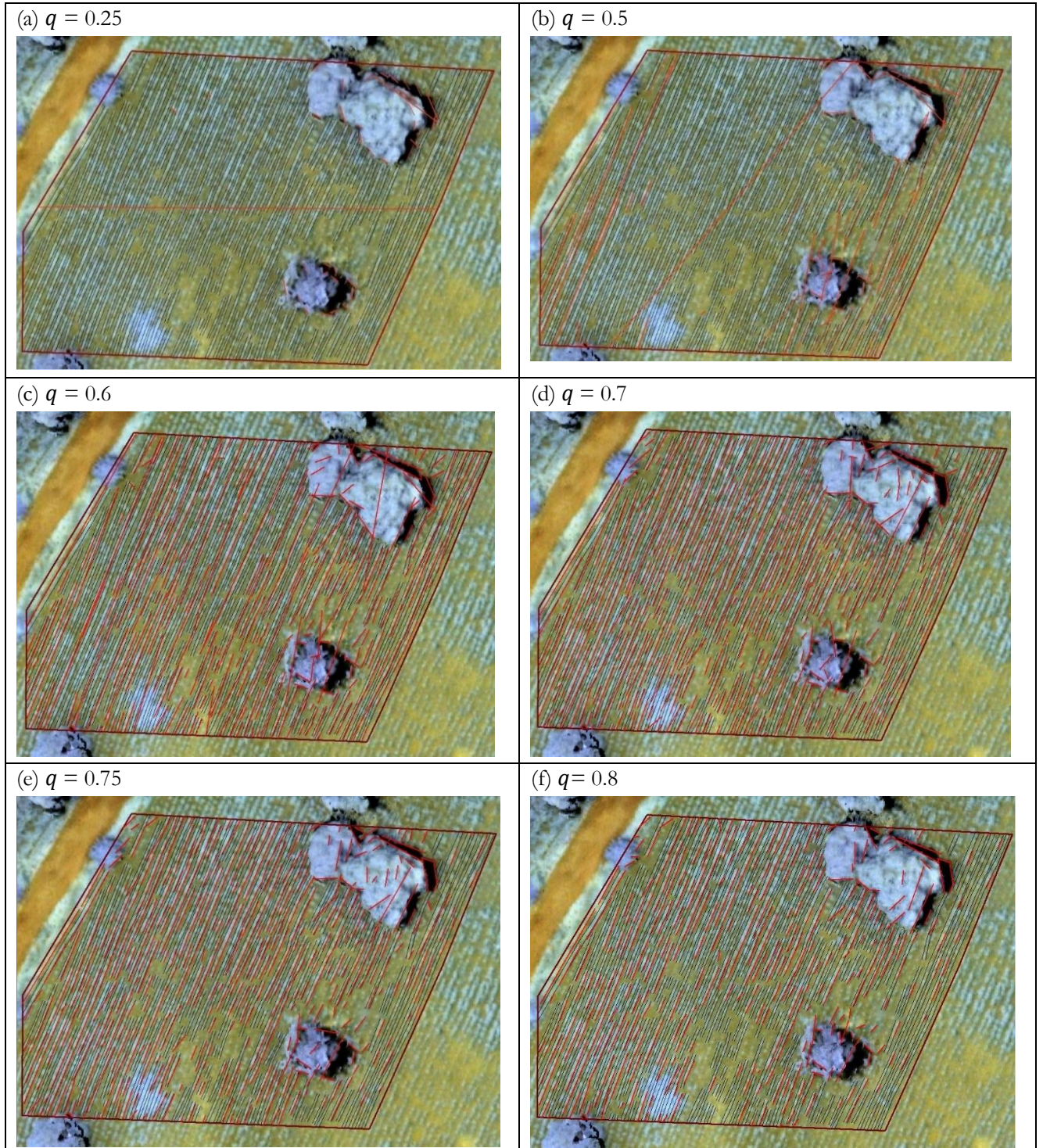
Figure 5.2: Crop row detection at different q parameter values. Black segments are the reference lines, red segments are the detected lines

5.1.3. Tuning of the angular tolerance for region growing (τ) parameter

The tuning of the τ parameter was done by maintaining the scale at $S = 0.8$ and the magnitude quantile at $q = 0.7$. The tuning the τ parameter was carried out for different values of $\tau = 5.625°$, $\tau = 11.25°$, $\tau = 22.5°$ and $\tau = 45°$. Epsilon was maintained at $\varepsilon = 1$ and the threshold for the smallest region area in pixels

maintained at 10 pixels. As observed in Figure 5.3, $\tau = 5.625°$ and $\tau = 11.25°$ produced so many line segments with many small pieces of segments along one edge while $\tau = 45°$ produced very few line segments with a lot of missed detections. $\tau = 22.5°$ (considered as the optimal τ value in this study) produced more correct line segments. There were few missed detections compared to $\tau = 45°$ and few and continuous line segments as compared to $\tau = 11.25°$.

(a) $\tau = 5.625°$	(b) $\tau = 11.25°$
(c) $\tau = 22.5°$	(c) $\tau = 45°$
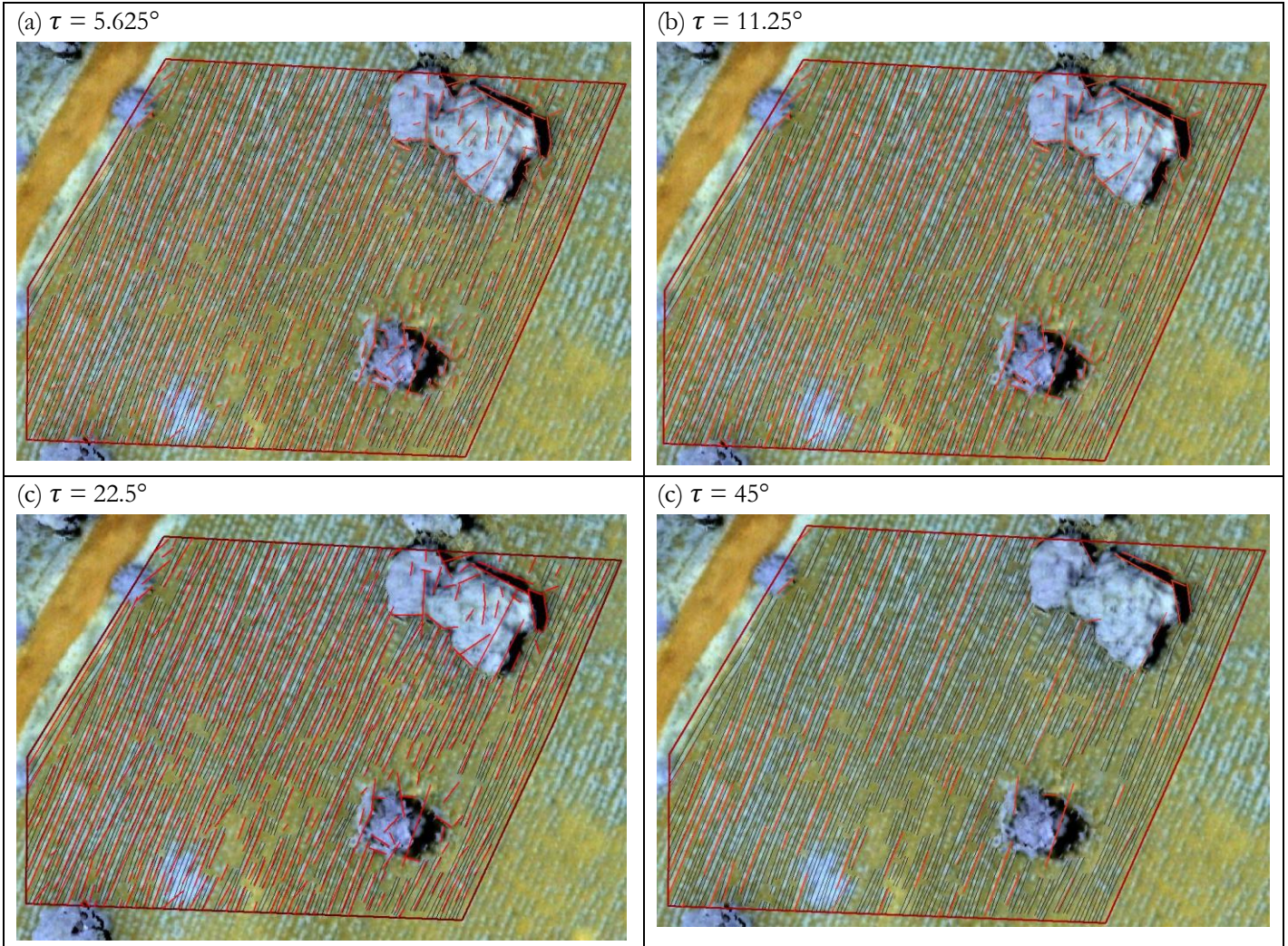
Figure 5.3: Crop row detection at different τ parameter values. Black segments are the reference lines, red segments are the detected lines

5.1.4. Tuning of the epsilon (ε) parameter

The ε parameter was tuned by maintaining the others at $s = 0.8$, $q = 0.7$ and $\tau = 22.5°$ respectively. The tuning of this parameter was done at different values of $\varepsilon = 0.1$, $\varepsilon = 0.5$, $\varepsilon = 1$, $\varepsilon = 5$ and $\varepsilon = 10$. The threshold for the smallest region area in pixels was maintained at 10 pixels. Figure 5.4 shows the results of UAV image at various ε parameters. The higher the value of ε tested, the more the number of line segments detected. This means that with a high value of ε, the more the number of detected lines are considered meaningful by the algorithm, even though they are not. $\varepsilon = 1$ was considered as the optimal value in this study.
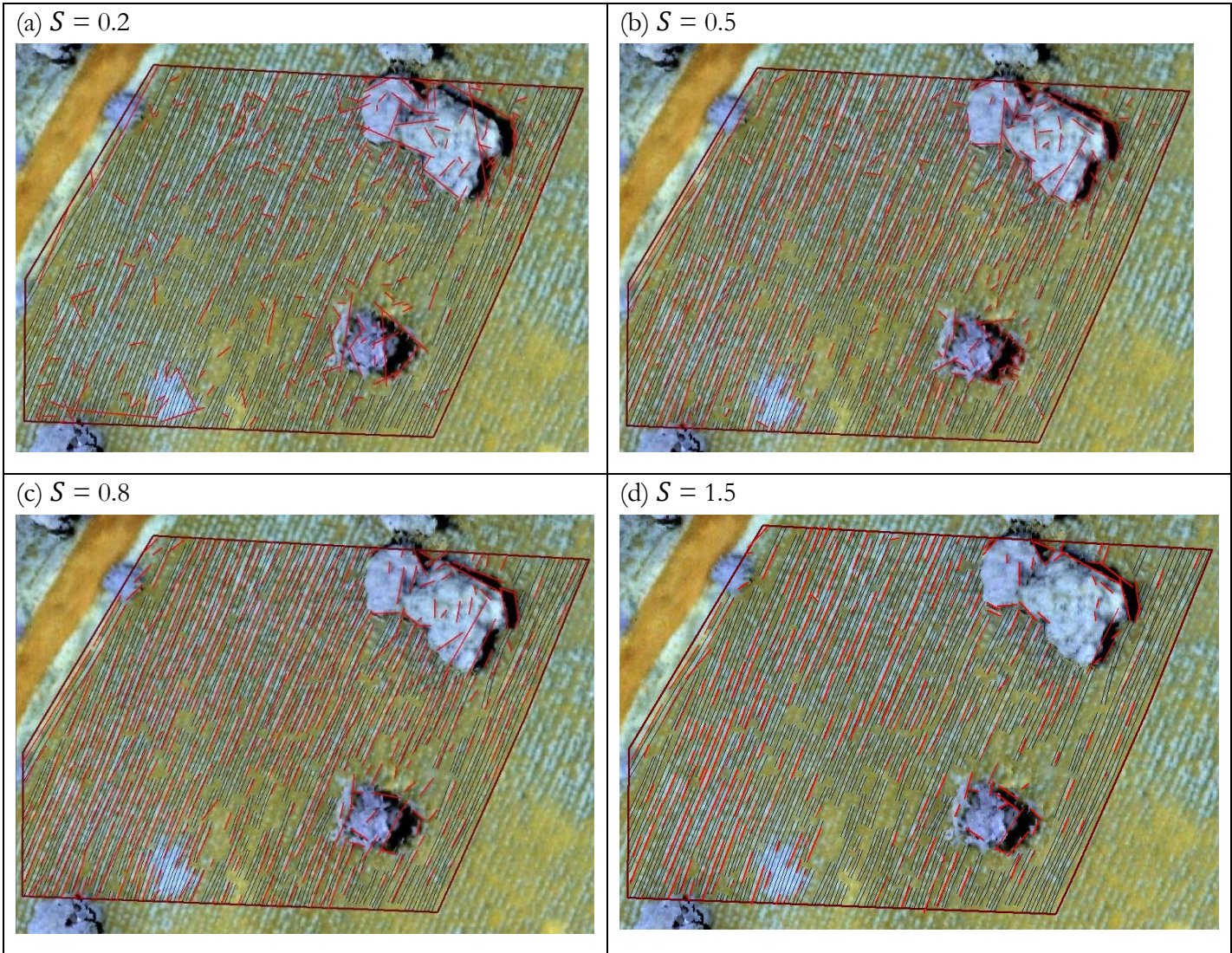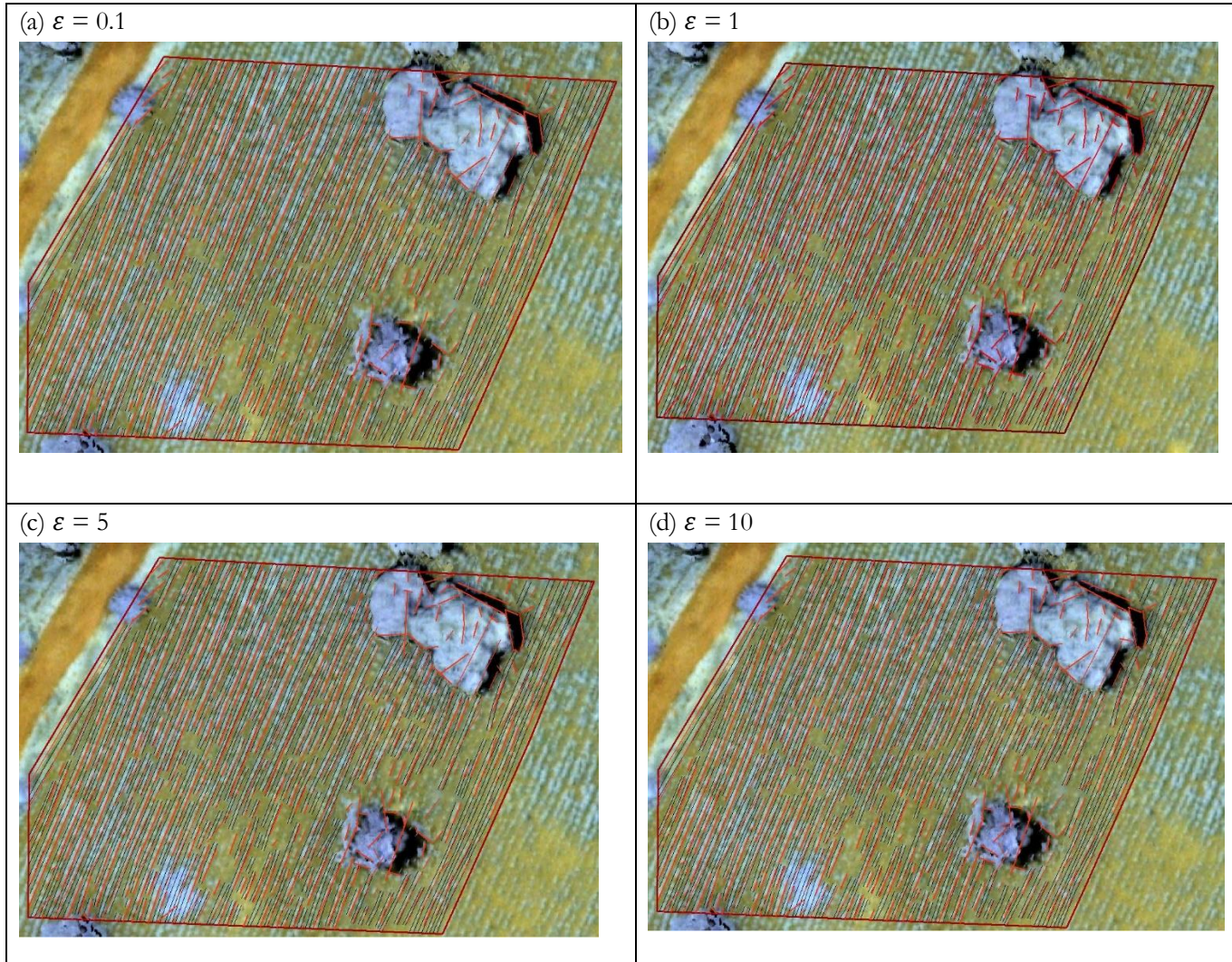
Figure 5.4: Crop row detection at different ε parameter. Black segments are the reference lines, red segments are the detected lines

5.1.5. Tuning of the threshold for the smallest region area parameter

The last parameter to be estimated was the threshold for the smallest region area in pixels. This parameter gives the threshold of detection for the minimum area in pixels. The estimation was done by maintaining the other parameters at $S = 0.8$, $q = 0.7$, $\tau = 22.5°$ and $\varepsilon = 1$. The different values estimated representing the number of pixels were; 0.5, 1, 10, 20 and 50. Figure 5.5 shows the results for the UAV image at various values tested.

At 0.5 pixels, very many lines were detected but only a few printed, only at the edges and top of trees. At 50 pixels, there were less rows detected with a lot of missed detections. Values between 1 and 20 produced similar results and therefore either of them could be used as an optimal value. The value of 10 pixels was selected as the optimal one to be used in this study.

(a) Minimum area = 0.5 pixel	(b) Minimum area = 10 pixels
(c) Minimum area = 20 pixels	(d) Minimum area = 50 pixels
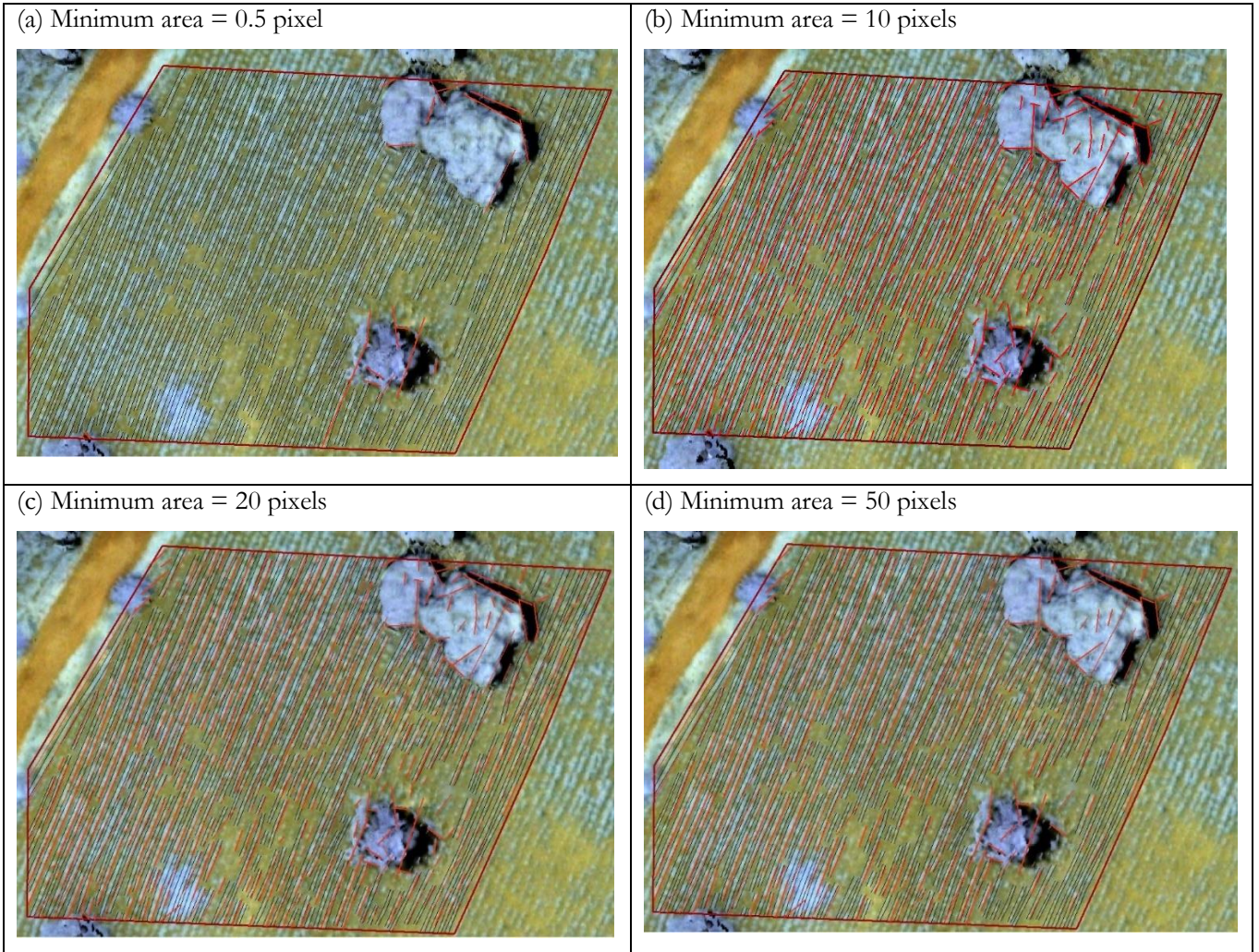
Figure 5.5: Crop row detection at different values of threshold for the smallest region area. Black segments are the reference lines, red segments are the detected lines

5.2. Approximating the undetected side of the crop rows

After estimating all the internal parameters of the algorithm, the optimal values selected were; $S = 8$, $q = 0.7$, $\tau = 22.5°$, $\varepsilon = 1$ and minimum area = 10 pixels. As discussed in Section 4.4. only one side of the crop rows was being detected by the algorithm. Therefore, the undetected side of the rows were approximated following the procedure explained in the same section. The orientation angles of the detected lines were calculated and represented in a histogram to help in interpretation of the results. The detected lines with highest peak on the histogram were selected as those representing crop rows while the ones outside this range were discarded. The approximated width of 0.5 m per crop row was then used to approximate the other side of the row. For UAV image subset of field 23 in cluster 3, most of the detected lines with the same orientation as the crop rows are between the range of 55° and 80° as observed in the left-hand side histogram in Figure 5.6. After discarding the ones outside this range, the result is as seen on the right-hand side histogram in Figure 5.6 and right hand side image in Figure 5.7. As observed in Figure 5.8 below, the approximation of the other side of the crop row at a distance of 0.5 m gave a clearer representation of crop rows in the field.
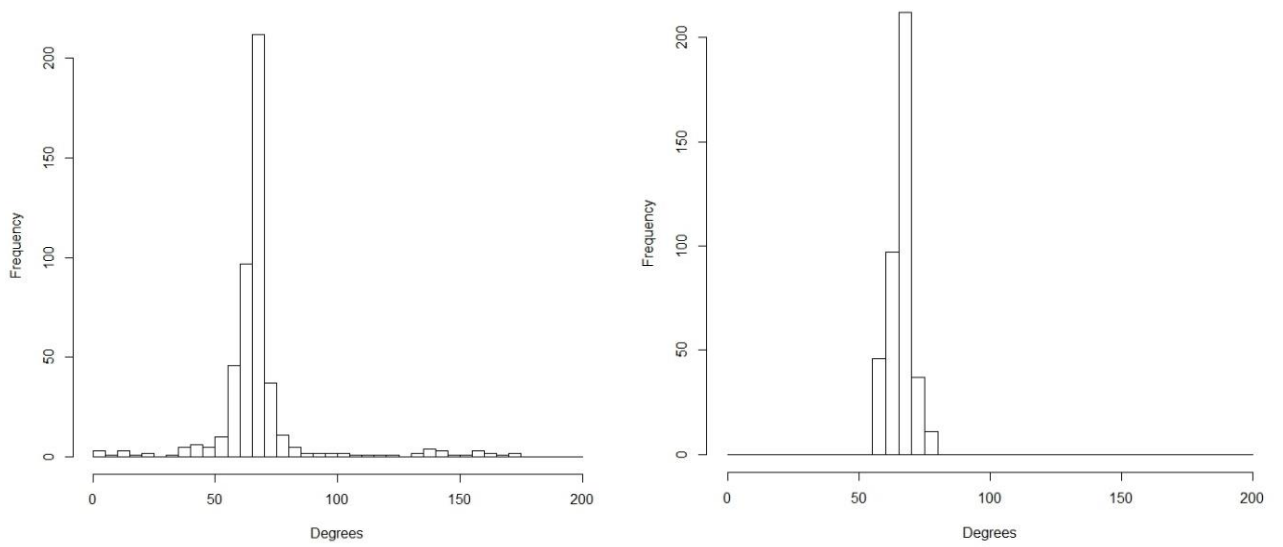
Figure 5.6: Histogram of crop row orientation. Left histogram is for all the detected rows, the right histogram is after discarding rows that have different orientation dominance as the crop rows
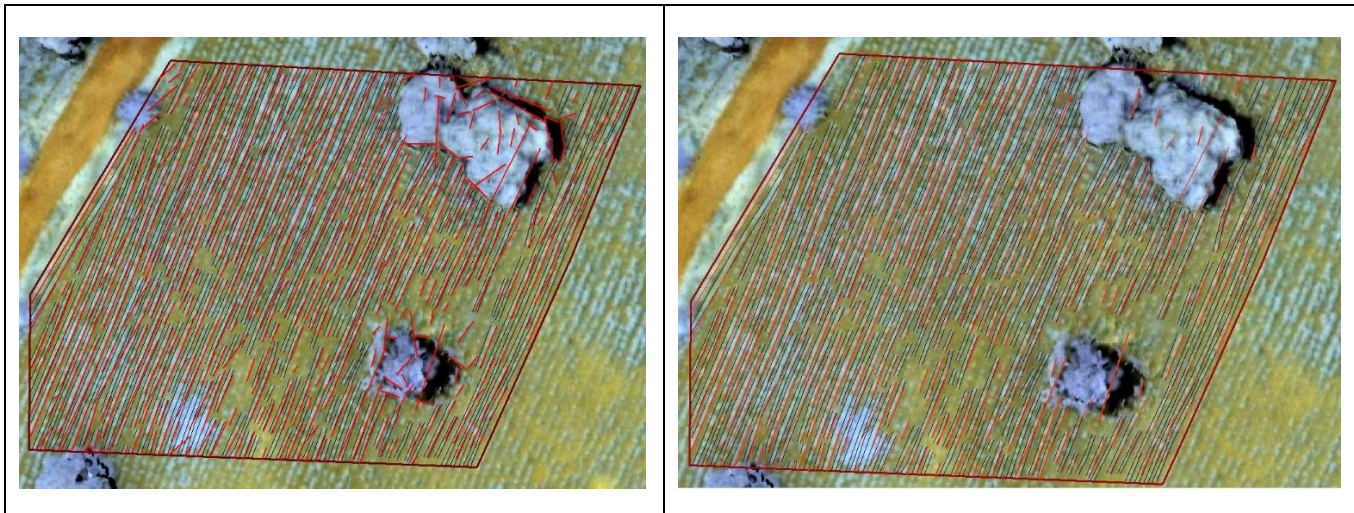
Figure 5.7: Orientation analysis. Left image shows all the detected lines while the right image shows the detected lines with same orientation as crop rows after discarding ones ouside the range of 55°- 80°. Black segments are the reference lines; red segments are the detected lines.
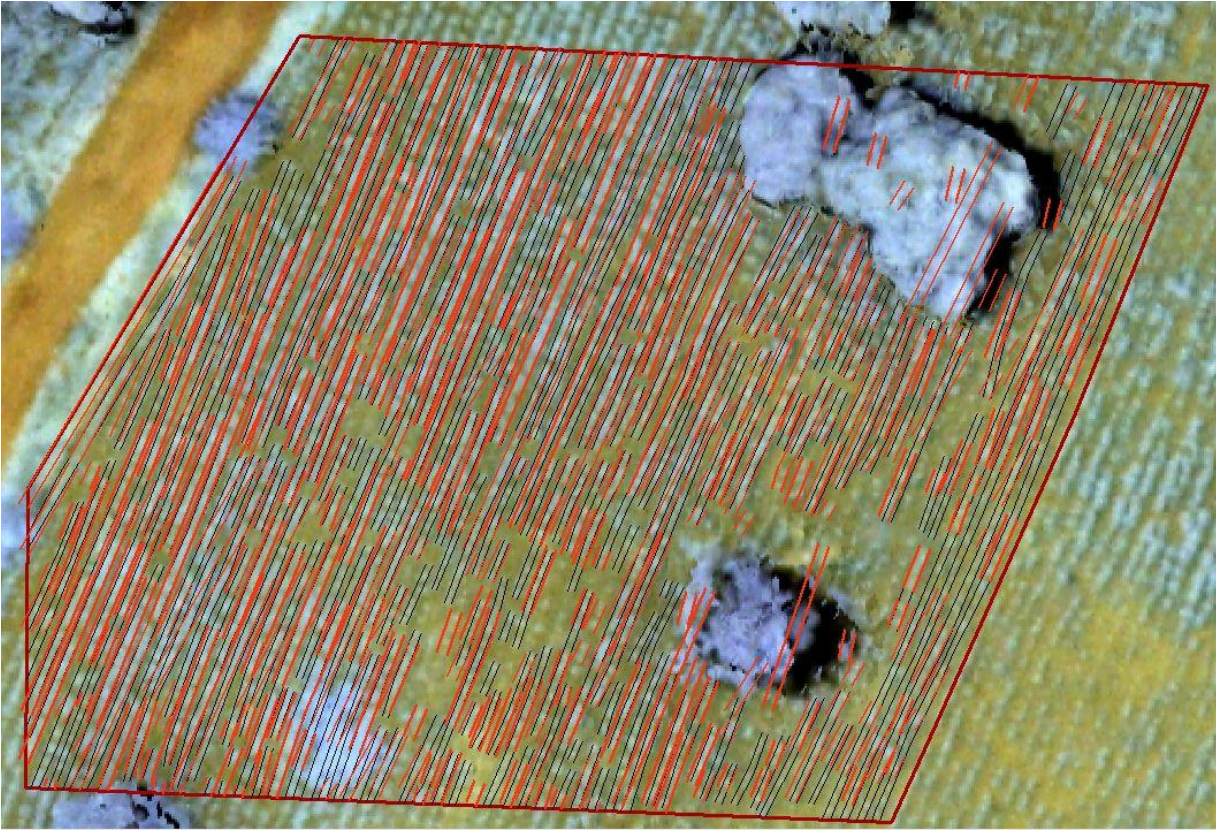
Figure 5.8: Result of approximating the undetected side of the row. Black segments are the reference lines, red segments are the detected lines

5.3.   LSD results on UAV images with texture features

The detection was carried out on UAV imagery with the texture features. The texture features were extracted at four directions (0°, 45°, 90° and 135°), d = 1, 2 and 3 for window size 3 x 3 and d = 1 for window size and 5 x 5 as discussed in Section 4.1. With the detection of crop rows using the texture features with UAV images there was no much difference observed between the different sets of texture features analysed. All the detected lines were mostly on the same positions as the detection without texture features. There were very slight differences in the number of detected lines for the various texture features, mainly due to some producing many line segments along one edge of the crop row while others having longer and less line segments along one edge of the crop row. Figure 5.9 shows results for various UAV images with texture features.
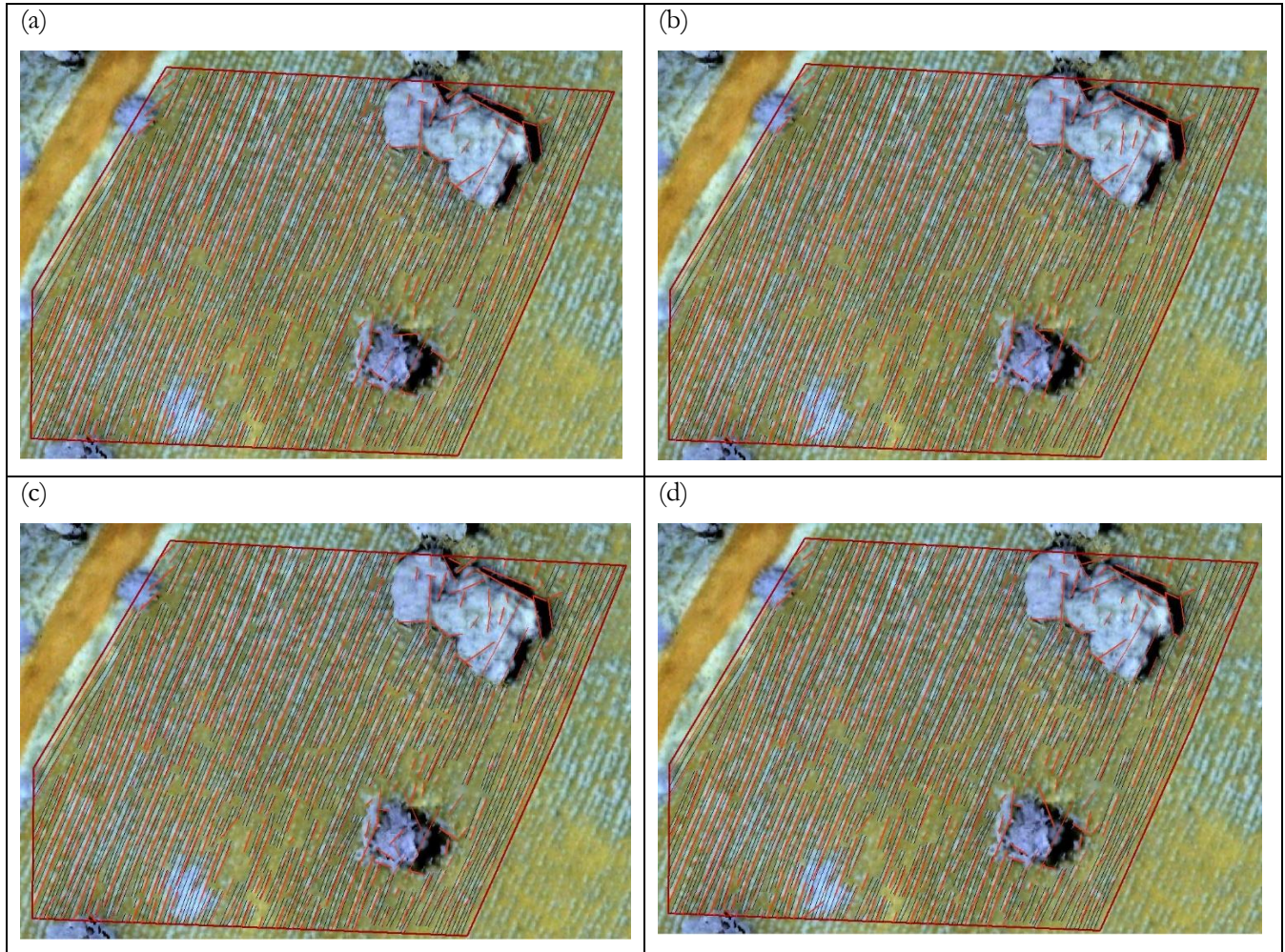
Figure 5.9: Result for crop row detection on UAV with texture features. (a) Texture features extracted at 0°, d = 1, using a 3 x 3 window size; (b) texture features extracted at 45°, d = 2, using a 3 x 3 window size; (c) texture features extracted at 135°, d = 3, using a 3 x 3 window size; (d) texture features extracted at 90°, d = 1, using a 5 x 5 window size. Black segments are the reference lines, red segments are the detected lines.

5.4.   Results for crop row detection for different dates

The detection of crop rows was carried out for the UAV images of the different dates between August and November. For subset 1, which is in cluster 3, the analysis was done for the 3 images August, September and October. There was no UAV image available for the month of November in this cluster. For subset 2, the analysis was done on 4 images between August and November.

The results generally showed more missed detections in the progressive months except for the October UAV image in for subset 1 where the detections were more successful than in the previous month September. The LSD results for subset 1 are as observed in Figure 5.10 while for subset 2 are presented in Figure 5.11.
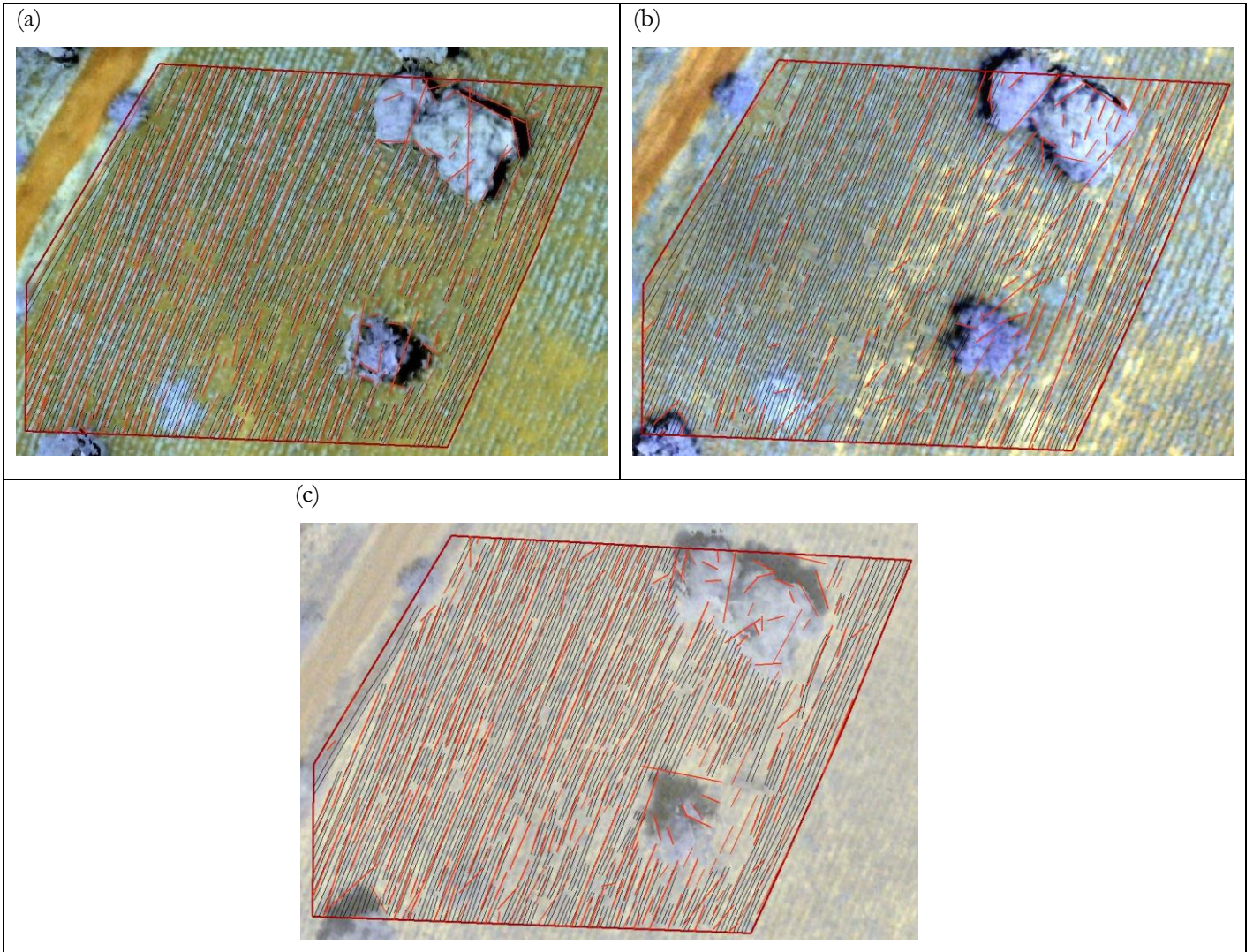
Figure 5.10: LSD results for different dates for subset 1 in cluster 3. (a) Result for UAV image dated 25/08/2014; (b) result for UAV image dated 18/09/2014; (c) result for UAV image dated 27/10/2014. Red lines are the detected lines while black lines are reference lines.
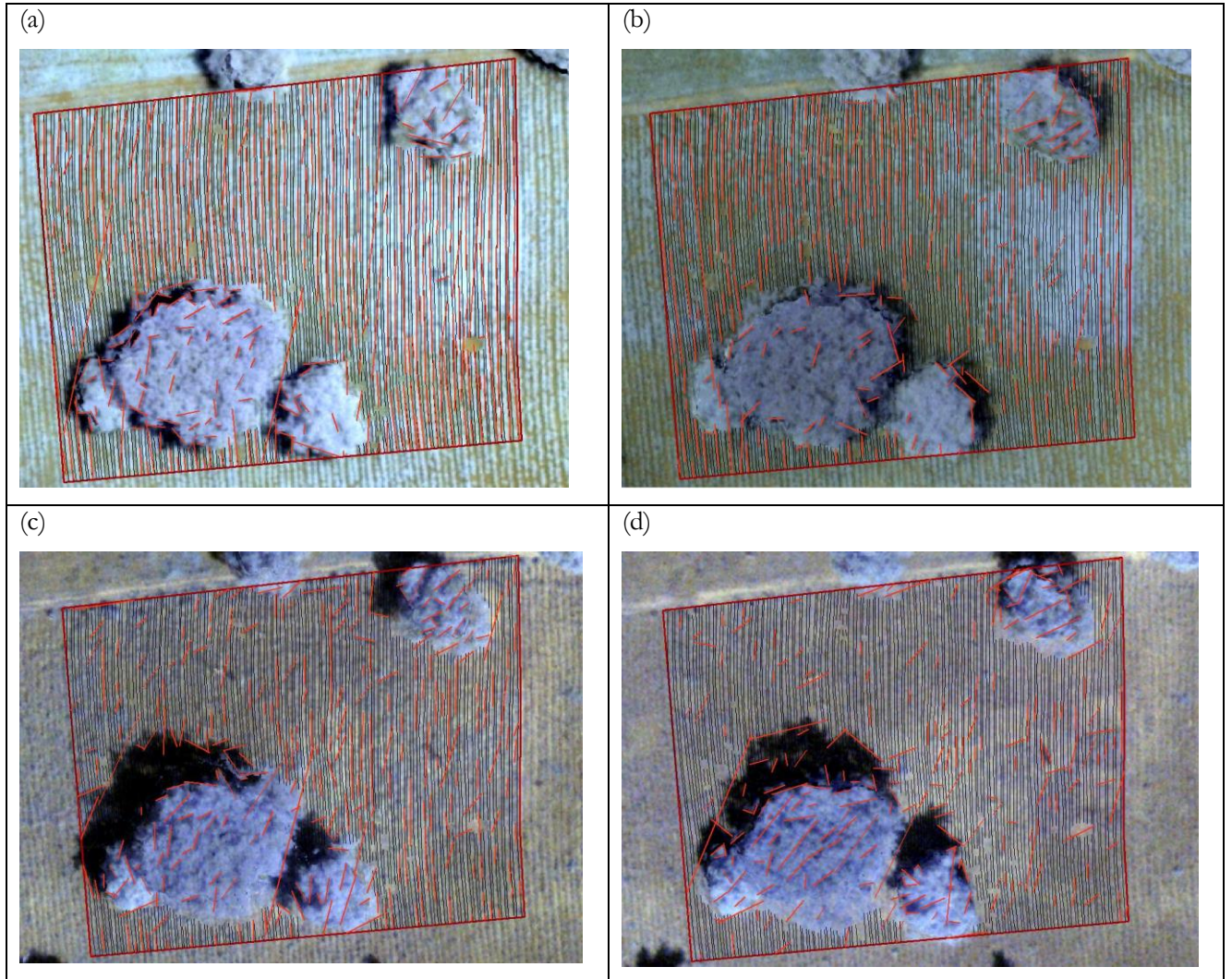
Figure 5.11: LSD results for different dates for subset 2 in cluster 4. (a) Result for UAV image dated 20/08/2014; (b) result for UAV image dated 11/09/2014; (c) result for UAV image dated 27/10/2014; (d) result for UAV image dated 26/11/2014. Red lines are the detected lines while black lines are reference lines.

The processing time for the LSD algorithm was also assessed to determine how efficient it is in terms of computation time. This was done on the two whole fields. The processing time for subset 1 is indicated in Section 5.1.1. The UAV image of 25th August was used for field 23 in cluster 3 and the UAV image of 20th August for field 18 in cluster 4. The results are recorded in Table 5.1.

Table 5.1: The LSD processing time recorded for the two fields using a PC with 2.40 GHz processor.

Field no.	Gradient computation	Region growing	NFA computation	Total time
23	1.53 seconds	2.78 minutes	45.19 minutes	48.12 minutes
18	2.53 seconds	4.28 minutes	60 minutes	64.31 minutes

5.5.   Crop row detection on Satellite imagery

The VHR satellite imagery was the last to be analysed for detection of the crop rows. Parameter tuning was first carried out following the same procedure as in the UAV images. This was done on the

WorldView-2 satellite image captured on 29th July 2014. For all the parameters tested, no set of them produced any successful results. The World-View 2 imagery, QuickBird dated 26th August 2014 and GeoEye-1 imagery dated 25th September 2014 were then analysed at the set of parameters; S = 0.8, q = 0.7, τ = 22.5°, ε = 1 and minimum area = 10 pixels as used on the UAV images. This was carried out on the two selected cotton fields, 23 in cluster 3 and 18 in cluster 4. Figures 5.12 and 5.13 show the results of the detection on the 3 satellite images for cotton fields 23 and 18 respectively. Detection of crop rows on the satellite imagery for Nigeria was also performed using same internal parameters as in Mali. This was done to compare the result to that obtained in satellite images for Mali. Figure 5.14 shows the result of crop row detection on the WV-2 panchromatic band for Nigeria.

As observed in the results, the detection of crop rows on the satellite images in Mali was not successful. This is mostly due to the nature of the farms in Mali. Although the resolution of the panchromatic band could be considered as a limiting factor to successful detection, this is contradicted by the detection result for Nigeria. As seen in Figure 5.14 and also in work by Alemu (2016), the analysis was on VHR satellite image (WV-2) in Nigeria; which have similar spatial and spectral characteristics as imagery used in Mali. The only difference is that the characteristics of farm fields in Nigeria are much different from Mali. The farms in Nigeria image appear to be well maintained, the crop rows are well spaced and have high densities of crops. This makes them more clear and easier to detect. On the other hand, crop rows as seen in Mali satellite imagery can barely be identified and are therefore hard to detect throughout the entire growing season. This could be mainly due to; poor spacing of the rows, low densities of the crops on the rows and lack of weeding resulting to weeds growing as tall as the crops; making it hard to be identify the crop rows.
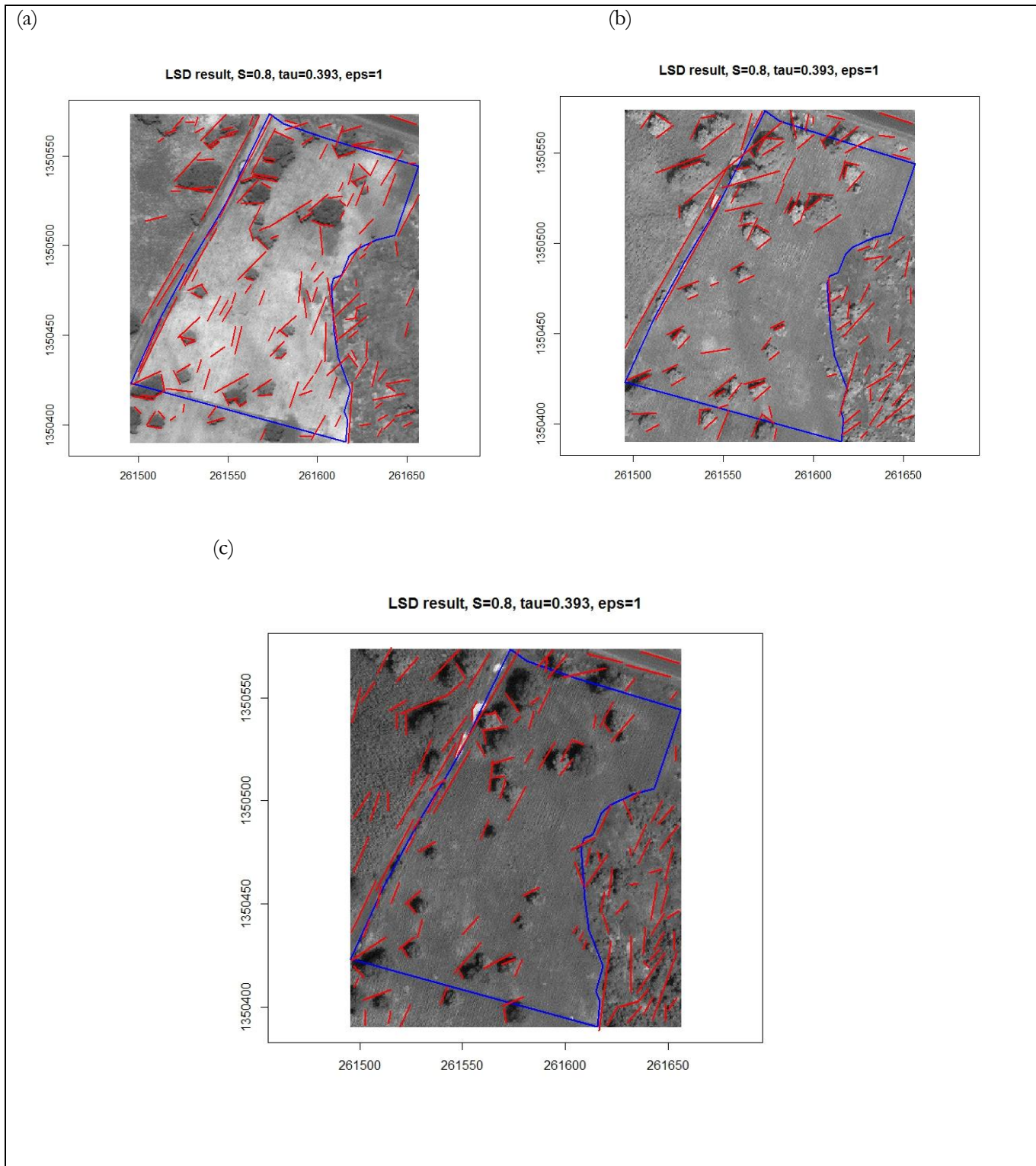
Figure 5.12: LSD results for VHR satellite images for cotton field 1. (a) Result for WorldView-2 satellite image; (b) result for QuickBird satellite image; (c) result for GeoEye-1 satellite image.
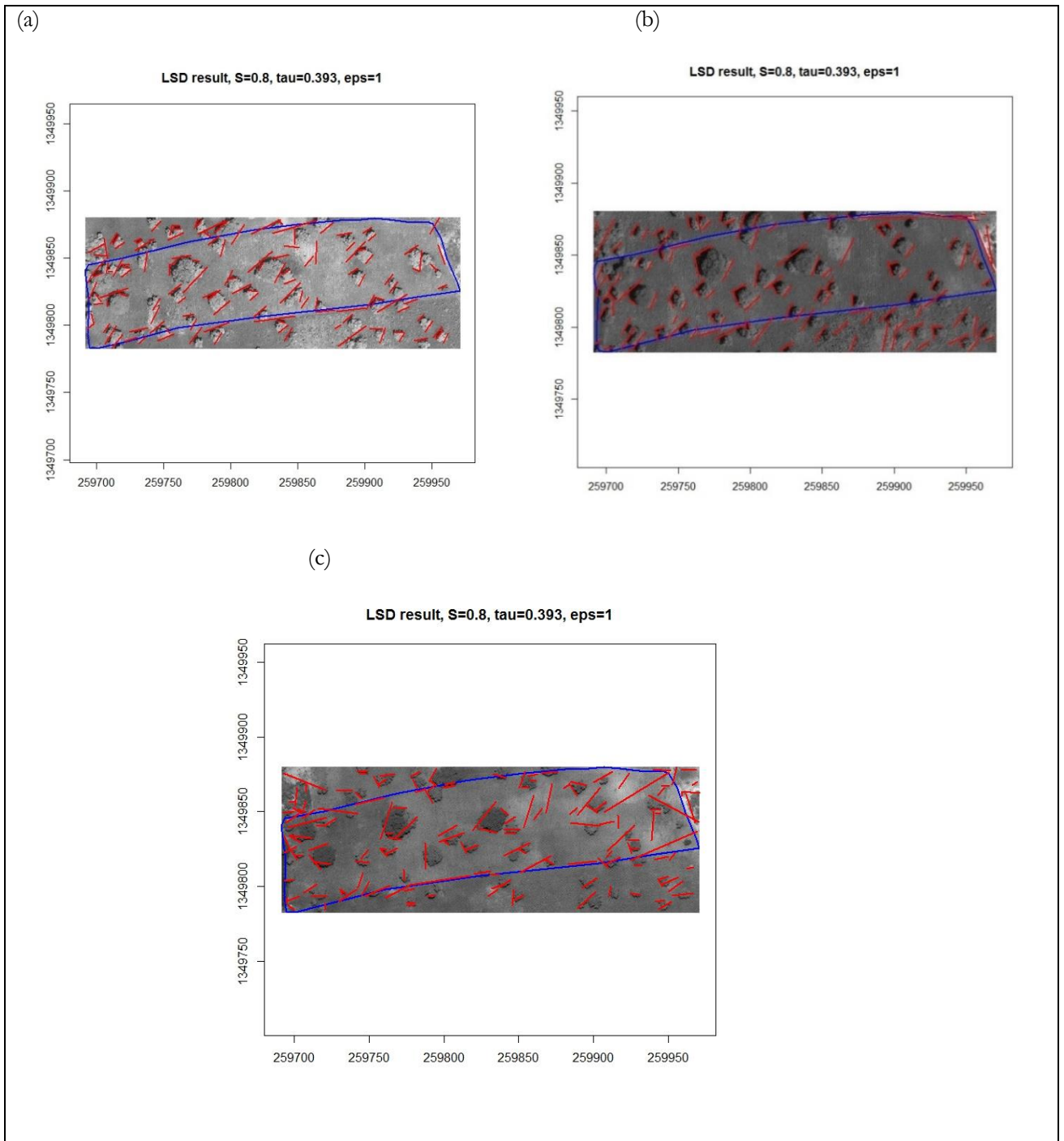
Figure 5.13: LSD results for VHR satellite images for cotton field 2. (a) Result for QuickBird satellite image; (b) result for GeoEye-1 satellite image; (c) result for WorldView-2 satellite image.

LSD result, S=0.8, tau=0.393, eps=1
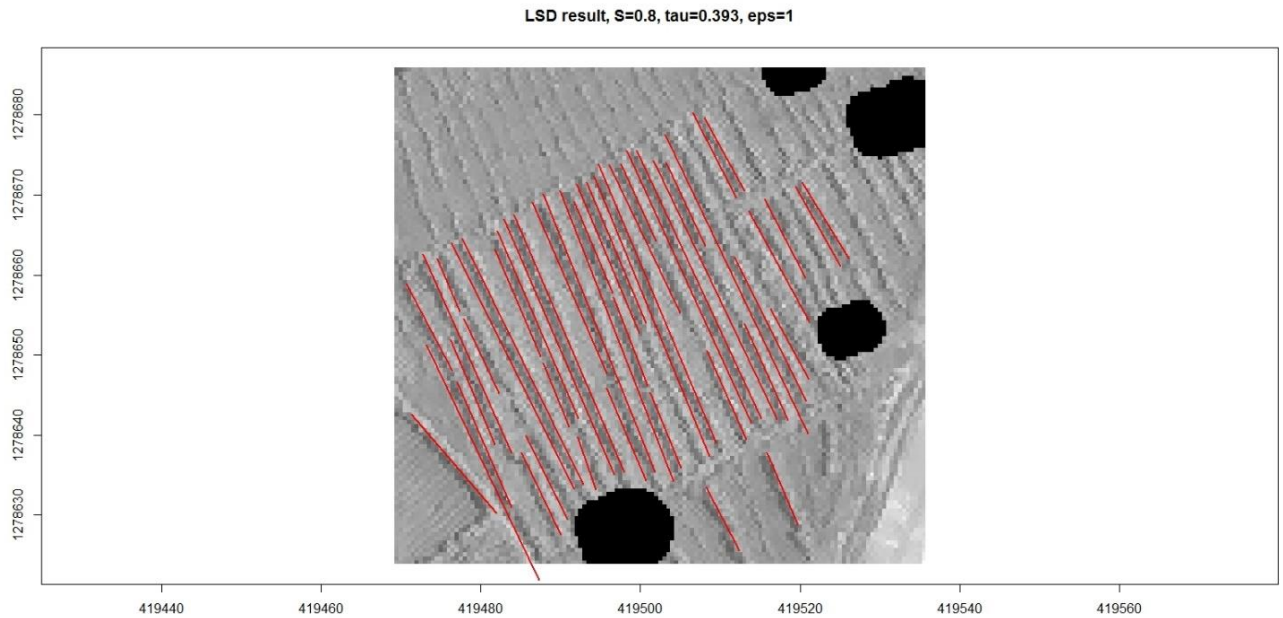
Figure 5.14: LSD result for crop row detection on WorldView-2 satellite image of Nigeria

5.6.   Validation of the crop row detection on UAV images

The validation was done by comparing the detected line segments with the digitized references rows. The orientation dominance of both the detected lines and the reference rows were assessed and graphically presented in rose diagrams. For the automatically detected lines, the orientation dominance was assessed after discarding the lines considered as not representing crop rows and approximating the undetected side of the crop row. Table 5.2 shows the results of the two subsets with the number of reference lines, detected lines, orientation angle in radians and the difference of orientation dominance between the reference rows and the detected rows. Subset 1 is for field number 23 in cluster 3 dated 25th August 2014 while subset 2 is for field number 18 in cluster 4 dated 20th August 2014. Figure 5.15 shows the rose diagrams of orientation dominance for the two subsets.

Visual inspection of the detected line segments was also done to assess how they compared to the manually digitized rows. It was observed that not all the crop rows in the fields were detected, although majority were. Most of the segments detected incorrectly were on top and along the edges of trees and also where there were large patches of weeds covering the crop rows. After discarding the lines that did not represent crop rows, the orientation dominance of the remaining line segments was observed to be similar to that of the manually digitized reference rows. The detected lines that represented the actual crop rows in the field for subset 1 were between 55° and 80° while subset 2 were between 80° and 100°.

Table 5.2: Orientation dominance of reference and detected line segments.

Subset	No. of lines		Orientation dominance (radians)		Difference in orientation dominance
	Reference	Detected	Reference	Detected	Difference in radians
1	312	686	1.18	1.15	0.03
2	272	648	1.62	1.59	0.03
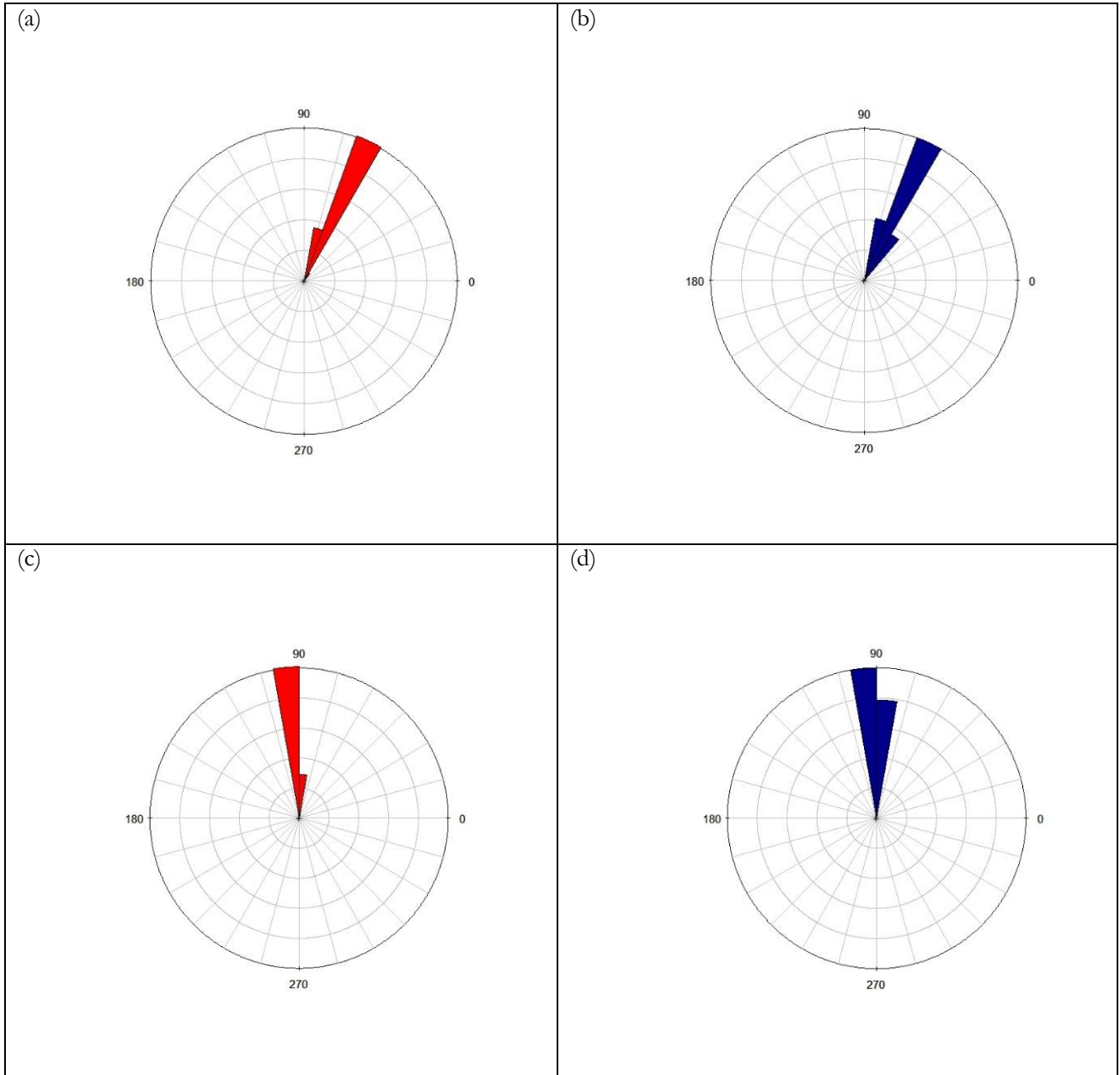
Figure 5.15: Rose diagrams showing orientation dominance of both reference lines and the detected lines; (a and c) = reference for subsets 1 and 2 respectively, (b and d) = detected for subsets 1 and 2 respectively.

5.7.   Results for weed detection

After the crop row detection analysis, weed detection was performed on the UAV images.

5.7.1.   Results for linear SVM

The tuning of the classifier was done by setting the algorithm in such a way that it picked the same training samples for each iteration when finding the best value of C. The Linear SVM was then predicted using the best value obtained. Figure 5.16 shows the classification results for the two subsets. The best value of C obtained after parameter tuning was 1 for both subsets 1 and 2.
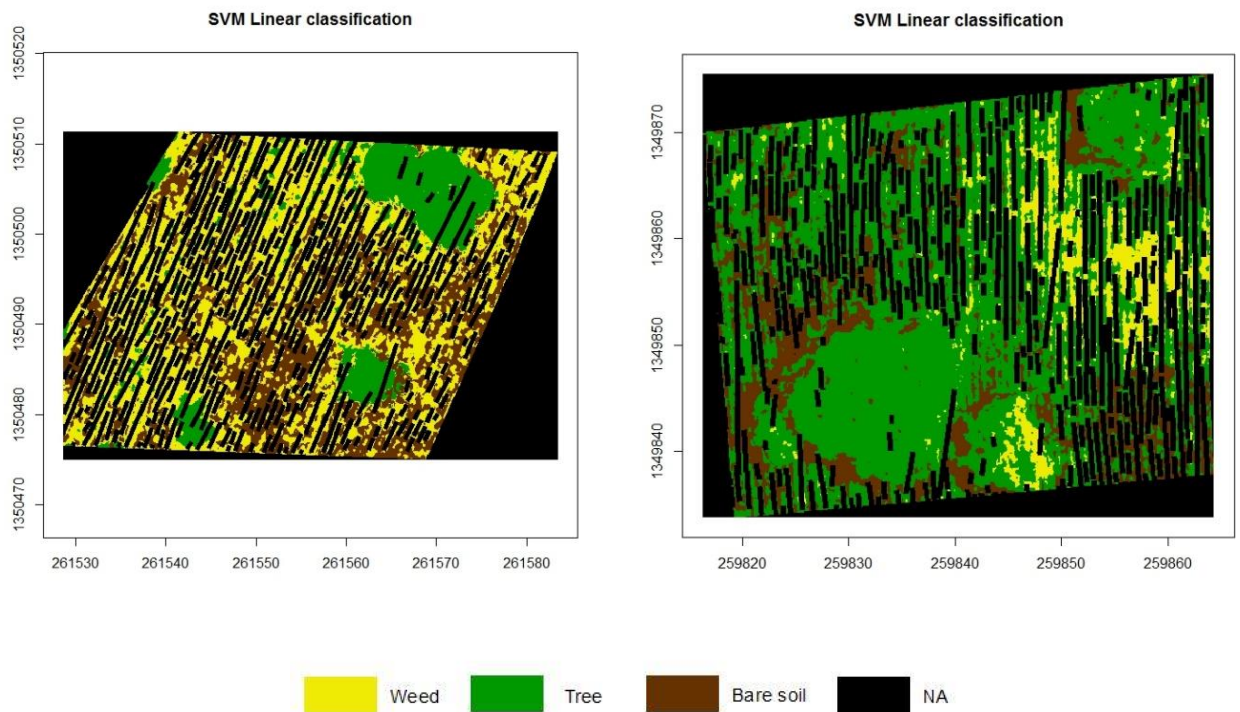
Figure 5.16: Results of Linear SVM. Left image is for subset 1 (Cluster 3 - 25th Aug 2014), right image is for subset 2 (Cluster 4 - 20th Aug 2014)

Linear SVM classification was observed to work better for the subset 1 image as compared to subset 2, although there was still confusion between the weed and tree classes. Subset 2 classification was very poor as observed in Figure 5.16. The confusion matrix in Table 5.3 shows the confusion between classes with most being between weeds and trees. The analysis was repeated by setting the algorithm not to pick the same training samples for each iteration while tuning for the best value of C. This was done to check if different training samples used to train the classifier at each iteration would have an effect on the classification results. The classification map result produced was the same, with best value of C obtained still being 1.

Table 5.3: Confusion matrix of subset 2 classification shows confusion between weed and tree classes

	Reference		
Class	Weed	Tree	Bare Soil
Weed	12	69	0
Tree	80	577	0
Bare Soil	0	0	104
NA	0	0	0

(Prediction — row label spanning the left column)

5.7.2. Results for RBF SVM

The tuning of the regularization parameter (C) and γ parameter was performed and the best values obtained were used to predict the RBF SVM. The best values of C and γ obtained after parameter tuning were 1 and 0.1 respectively for both subsets 1 and 2. Due to confusion between the weed and tree classes as also observed in the case of Linear SVM, the classification was poor for subset 2. Both weed and tree classes were classified as weeds as observed in the right-hand side image in Figure 5.17. The tuning of parameters was repeated for subset 2 without fixing the same training samples during each iteration of finding best values. The best value of C and γ obtained were still the same at 1 and 0.1 respectively. There was no observed improvement in the classification results.
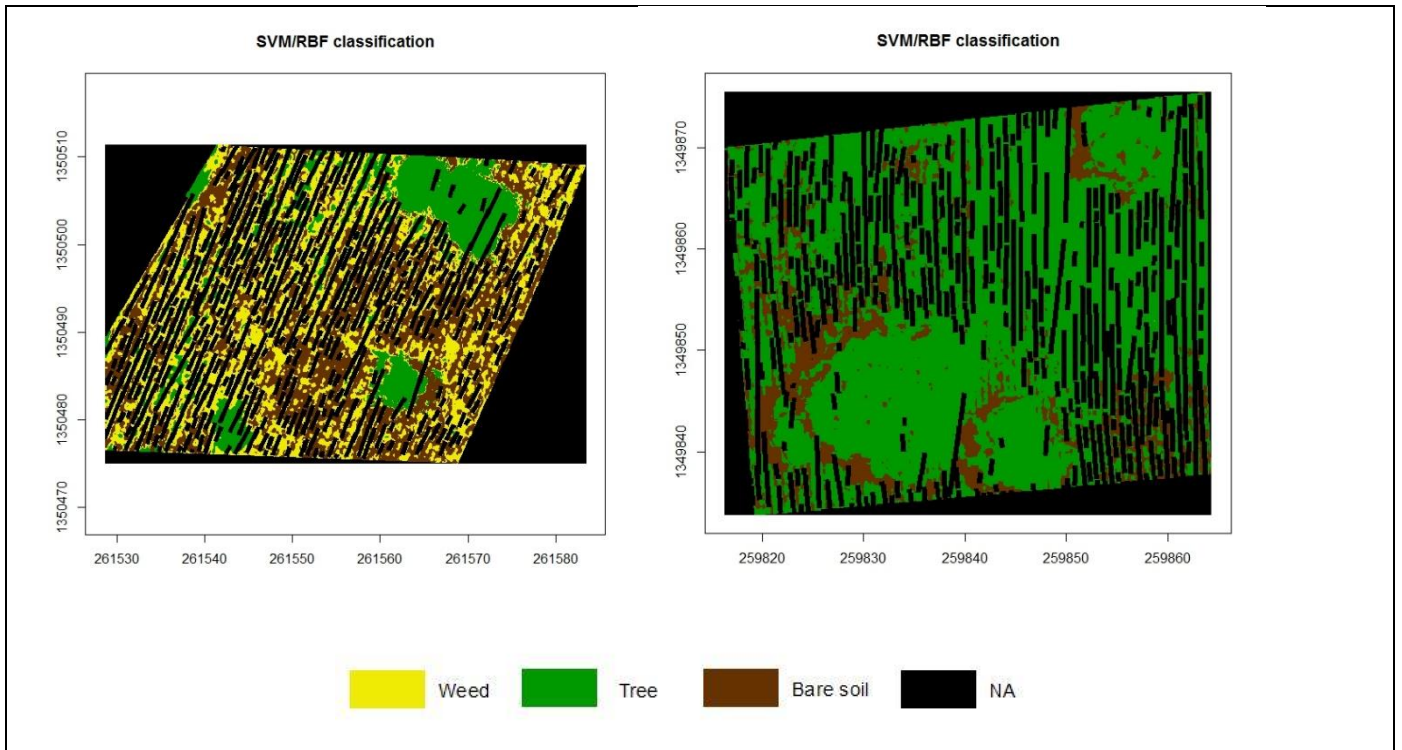
Figure 5.17: Results of RBF SVM. Left image is for subset 1 (Cluster 3 - 25th Aug 2014), right image is for subset 2 (Cluster 4 - 20th Aug 2014)

5.7.3. Results for linear and RBF SVM after masking of trees

As discussed in Section 4.6.5, manual masking of trees was done due to the errors in the classification brought about by confusion between weed and tree classes. This was then followed by tuning the classifier excluding the tree class. After tuning of the parameters, best values of C obtained for Linear SVM was 1, while best values of C and γ for RBF SVM was 1 and 0.1 respectively for both subsets 1 and 2. As observed in Figures 5.18 and 5.19, the masking of trees helped in improving the classification maps of the two subsets.
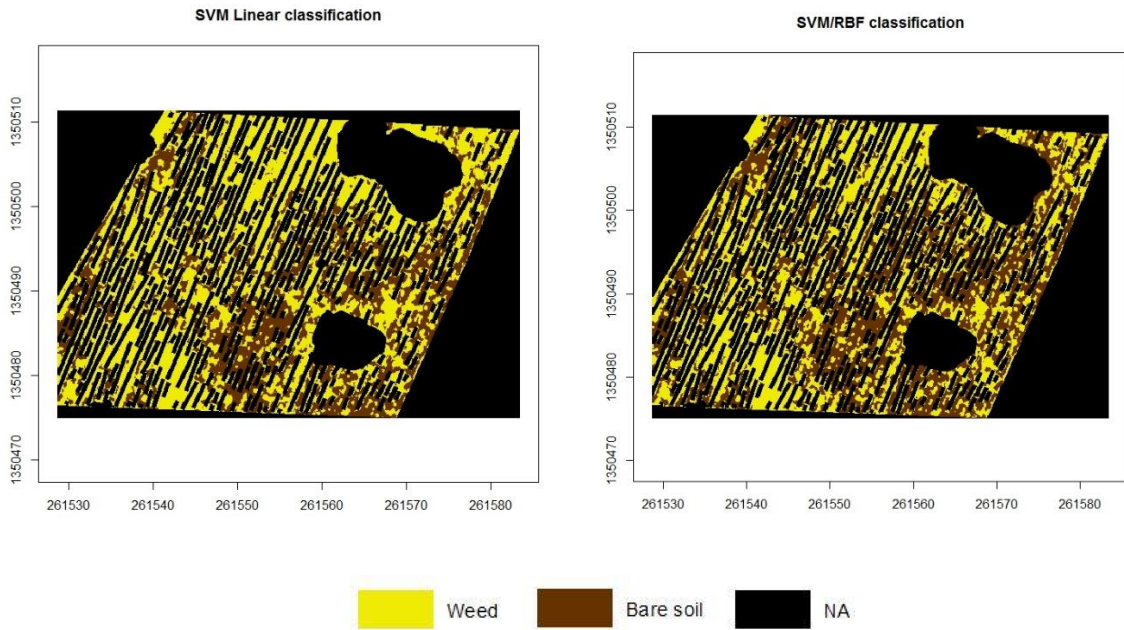
Figure 5.18: Linear and RBF SVM classification results of subset 1 after masking out trees
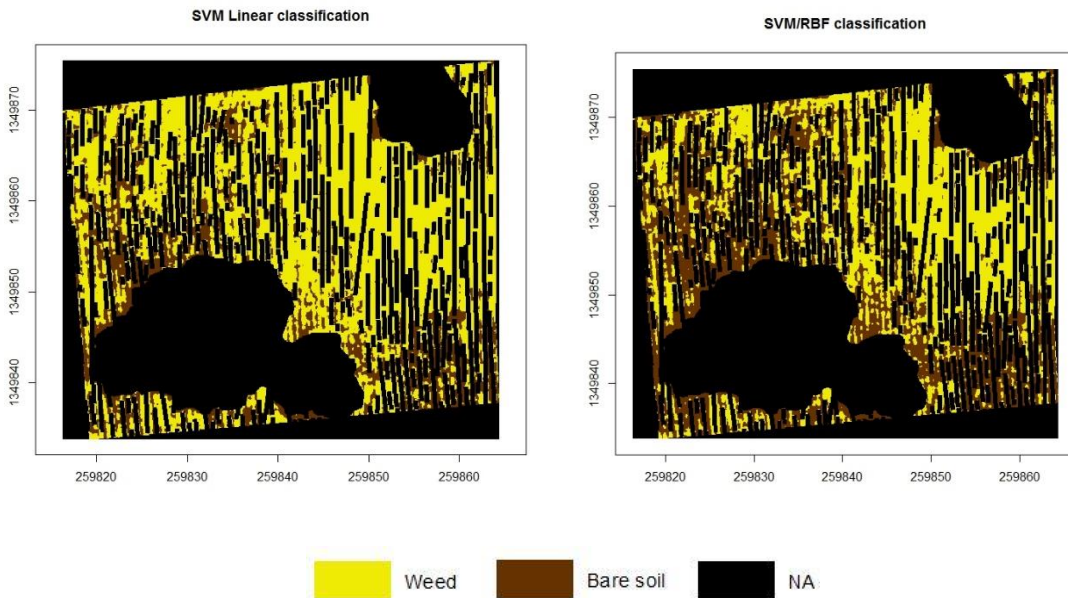
Figure 5.19: Linear and RBF SVM classification results of subset 2 after tree masking

5.7.4. Results for linear and RBF SVM on UAV images with texture features

The final analysis of the weeds was carried out on UAV images with texture features. The classification was done after tuning the best value of C for the Linear SVM and best values of C and γ for the RBF SVM. The classification results of analysis on texture features extracted at 0°, d = 1, on a 3 x 3 window; and features extracted at 90°, d = 1, on a 5 x 5 window size are presented in Figures 5.20 and 5.21 respectively. The best C obtained for Linear SVM in the 3 x 3 window size was 1 while best C and γ obtained for RBF SVM was 18.33 and 0.264 respectively. For window size 5 x 5, best C obtained for Linear SVM was 37.93 while best C and γ in RBF SVM was 1 and 0.1 respectively. The texture features did not help in improving the classification result but rather the results appeared to get worse than those of images without texture features.
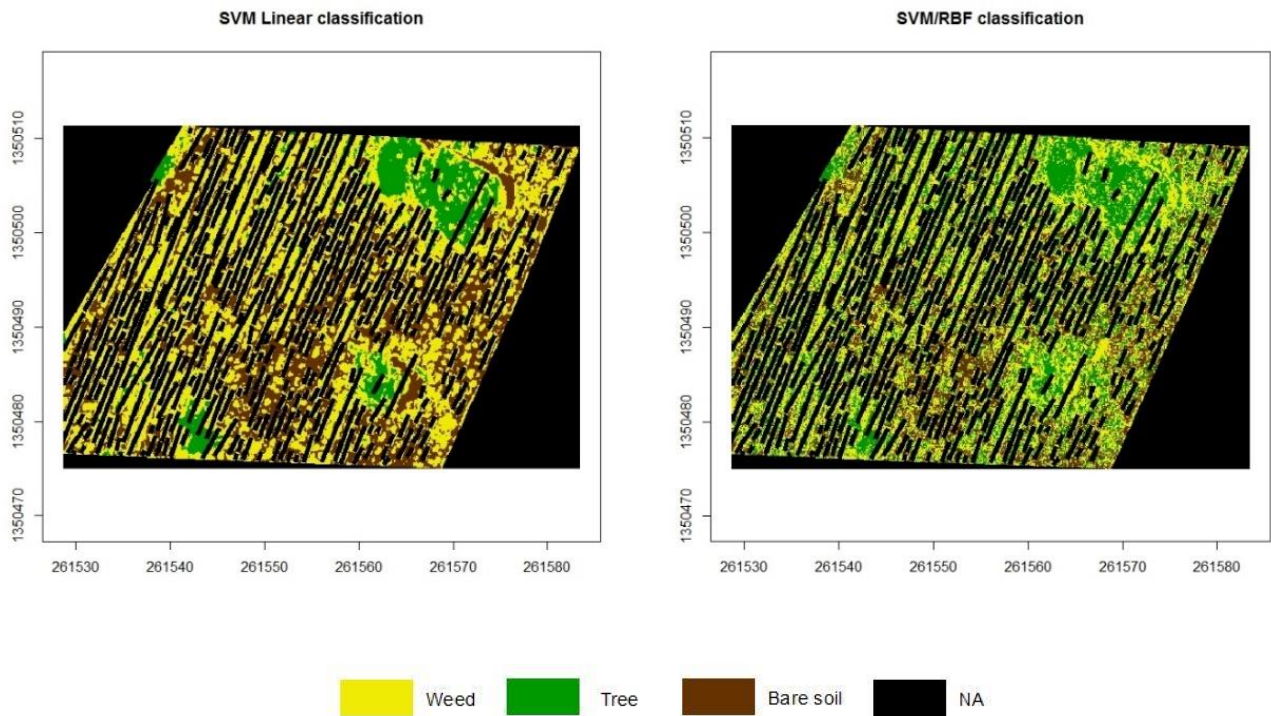
Figure 5.20: Linear and RBF SVM on images with texture features at 0° orientation, d=1 on a 3 x 3 window size.

Table 5.4: Confusion matrix of subset 1 with texture features at 0° orientation, d=1 on a 3 x 3 window size.

		Reference		
	Class	Weed	Tree	Bare Soil
Prediction	Weed	123	60	34
	Tree	114	364	0
	Bare Soil	0	0	283
	NA	0	0	0
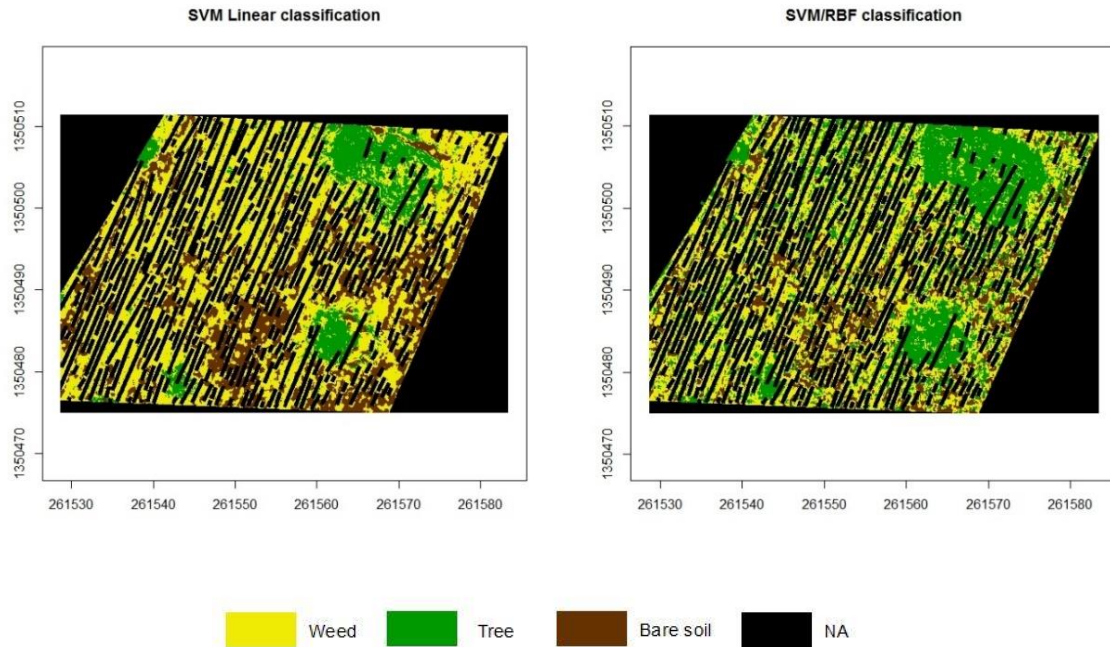
Figure 5.21: Linear and RBF SVM on images with texture features at 90° orientation, d=1 on a 5 x 5 window size.

Feature selection was then performed for all the sets of GLCM features extracted. This was not meaningful as for all the GLCM features, the best selected features were bands 2 and 3 except for GLCM features extracted at 135°orientation which gave best features as 1 and 3. This means that no GLCM texture feature was considered as useful by the algorithm, as the selected features are not texture features but the bands in the UAV image.

5.8. Results for weed analysis for different dates

The weeds analysis was performed on the two fields for different dates between August and November. This was done by applying SVM classifier on the whole field and not the subset. For field number 23 in cluster 3, three images were analysed, one each month between August and October. There was no UAV image available for the month of November in this cluster. For field number 18 in cluster 4, four images were analysed, one every month from August to November. The results of the weeds percentage cover, overall accuracy and Kappa coefficient values obtained are as presented in Tables 5.5, 5.6, 5.7 and 5.8

The analysis in field 23 showed increasing weed cover percentage every month. The September results for both Linear SVM and RBF SVM on the field with trees showed reduced weed percentage cover as seen in Tables 5.5 and 5.6. This is mainly because of confusion between weed and tree classes, hence, most weeds being classified as trees. The increase in the weeds from August to October as clearly seen in analysis of weeds after masking of the trees could be as a result of lack of weeding by farmers. This is because weeding in this field was done only once throughout the entire growing season as discussed in Section 3.2.3.

Table 5.5: Linear SVM results for percentage weed cover, overall accuracy and kappa for cotton field number 23 in cluster 3 with and without trees at different dates.

With trees	Date	Weed cover (%)	Overall Accuracy (%)	Kappa
23	25/08/2014	31.49	97	0.95
23	18/09/2014	6.19	82	0.68
23	27/10/2014	47.06	97	0.94
Without trees				
23	25/08/2014	43.06	98	0.96
23	18/09/2014	46.56	100	1
23	27/10/2014	49.92	99	0.99

Table 5.6: RBF SVM results for percentage weed cover, overall accuracy and kappa for cotton field number 23 in cluster 3 with and without trees at different dates.

With trees	Date	Weed cover (%)	Overall Accuracy (%)	Kappa
23	25/08/2014	17.37	85	0.70
23	18/09/2014	4.79	82	0.68
23	27/10/2014	20.75	90	0.75
Without trees				
23	25/08/2014	38.00	99	0.99
23	18/09/2014	46.41	100	1
23	27/10/2014	48.97	99	0.99

The analysis in field 18 also showed an increasing weed cover percentage every month. The result for the 11th September 2014 for the RBF SVM on the field with trees showed reduced weed percentage cover as seen in Table 5.7. This was mainly due to confusion between weed and tree classes and hence, most weeds were classified as trees. The results for the months of October and November show very high weeds percentage cover. Even though the increase could be true as no weeding is done in this field throughout the entire growing season as discussed in Section 3.2.3, the increase is also attributed to poor results in detection of crop rows where very few crop rows were detected in the UAV images of these two dates. Therefore, some of the pixels classified as weeds represent the missed crop rows on the ground.

Table 5.7: Linear SVM results for percentage weed cover, overall accuracy and kappa for cotton field number 18 in cluster 4 with and without trees at different dates.

With trees	Date	Weed cover (%)	Overall Accuracy (%)	Kappa
18	20/08/2014	25.20	88	0.78
18	11/09/2014	24.87	89	0.78
18	27/10/2014	72.03	96	0.90
18	26/11/2014	69.59	95	0.88
Without trees				
18	20/08/2014	27.37	100	1
18	11/09/2014	36.64	100	1
18	27/10/2014	72.67	100	1
18	26/11/2014	72.01	100	1

Table 5.8: RBF SVM results for percentage weed cover, overall accuracy and kappa for cotton field number 18 in cluster 4 with and without trees at different dates.

With trees	Date	Weed cover (%)	Overall Accuracy (%)	Kappa
18	20/08/2014	25.13	83	0.68
18	11/09/2014	4.74	87	0.73
18	27/10/2014	72.50	95	0.87
18	26/11/2014	66.41	95	0.87
Without trees				
18	20/08/2014	25.32	100	1
18	11/09/2014	34.85	100	1
18	27/10/2014	73.07	100	1
18	26/11/2014	76.54	100	1

5.9. Validation of weed detection

Accuracy assessment of the weeds analysis was done by looking at the overall accuracy and the kappa values obtained. These two did not give the true picture of the actual results. This is because some classification maps showed very poor results but their overall accuracy and kappa coefficient values obtained were still high depending on how the classes were classified. A good example is the result for subset 2 in Figures 5.16 and 5.17 which gave high overall accuracy (95%) and kappa (0.82) yet the classification map showed poor results. Also, as observed in Tables 5.5 and 5.6 on the analysis of weeds on the whole field with trees, the image of 18th September 2014 produced low weed cover percentage but the overall accuracy and the kappa values were still at the acceptable range. The same was observed in the classification results for RBF SVM for field 18 on 11th September as indicated in Table 5.8

The classification maps after masking of trees showed improved results; the overall accuracy for subset 1 and 2 for Linear SVM being 99% and 100% respectively and kappa values being 0.9 and 1 respectively. Overall accuracy in RBF SVM result was 99% for subset 1 and 95% for subset 2. The kappa was 0.99 for subset 1 and 0.98 for subset 2. This was also observed in results of weed analysis on the whole fields.

The weeds percentages calculated in the SVM classifier were then checked with the field reference data available. This data was measured between 15th August[t] to 17th September 2014 and therefore, only results

analysed for the two months could be compared. According to the reference data, the weed cover for both fields were ranging between 10 – 50%. The percentage cover results for field 23 calculated from the image in August were, for Linear SVM, 31.49% and 43.06% for analysis with trees and without trees respectively as seen in Table 5.5 and RBF SVM, 17.37% and 38.00% for analysis with trees and without trees respectively as seen in Table 5.6. This agreed with the range recorded in the reference data. The results for RBF SVM with trees was much lower than without trees due to most weeds being classified as trees. The percentage cover results for same field for the image of September were, for Linear SVM, 6.19% and 46.56% for analysis with trees and without trees respectively as seen in Table 5.5 and RBF SVM, 4.79% and 46.41% for analysis with trees and without trees respectively as seen in Table 5.6. The classification with masked trees agreed with the range recorded in the reference data.

The percentage cover results for field 18, calculated from the image in August were, for Linear SVM, 25.20% and 27.37% for analysis with trees and without trees respectively as seen in Table 5.7 and RBF SVM, 25.13% and 25.32% for analysis with trees and without trees respectively as seen in Table 5.8. This agreed with the range recorded in the reference data. The percentage cover results for same field for the image of September were, for Linear SVM, 24.87% and 36.64% for analysis with trees and without trees respectively as seen in Table 5.7 and RBF SVM, 4.74% and 34.85% for analysis with trees and without trees respectively as seen in Table 5.8. The classification with masked trees for SVM RBF and both Linear with and without trees agreed with the range recorded in the reference data. The field photos capture at different quadrats were also checked to see if they showed presence of weeds in the fields. Figure 5.22 shows field photos captured in field 23

Figure 5.22 Photographs captured in field 23 showing presence of weeds in the field. Source: STARS & ICRISAT (2014)

6. DISCUSSION

In this study, the main focus was applying the LSD and SVM algorithms on a real problem of crop row and weed detection in Mali, Africa. This was done by analysing two sets of imagery, the UAV imagery and VHR satellite imagery. The study involved the detection of crop rows on two cotton fields after which the weeds were detected between the rows. The crop rows were then validated by use of manually digitized crop row edges while the weeds accuracy assessment was done by visual inspection of classification map results, overall accuracy and kappa values obtained. The weeds analysis results were also validated using the reference data provided by the STARS project in collaboration with ICRISAT Mali.

6.1. Crop row detection

The LSD algorithm takes in one feature as an input for analysis. In this study, all the 3 bands of the UAV images were used in the analysis by getting their mean. This was important as, having more spectral information from the different bands help in improving the detection results. For the crop row detection using the VHR satellite imagery, the panchromatic band was used.

6.1.1. Crop row detection on the UAV images

The analysis started with parameter tuning where the various internal parameters were tuned before selecting the set of the most optimal ones to be used in the analysis. These included the scale (S), angular tolerance for region growing (τ), magnitude quantile for gradient thresholding (q), epsilon (ε) and the threshold for the smallest region area in pixels. The optimal results selected include $S = 0.8$, $\tau = 22.5°$, $q = 0.7$, $\varepsilon = 1$ and minimum region in pixels = 10. The parameter values of S, τ, and ε agreed to those in the study by Grompone Von Gioi et al. (2012). The gradient magnitude thresholding used is quantile based as discussed in Section 4.2.3. In studies by Grompone Von Gioi et al. (2012); Alemu (2016); Akinlar & Topal (2011), the threshold ω_q is set in order to eliminate the points that have an angle error bigger than the angle tolerance. This is done by setting maximum quantization error at 2 which is divided by the angle tolerance τ to get the magnitude threshold.

An algorithm should not be termed as efficient if it only produces accurate detections, but there are other factors to be considered. The LSD algorithm was assessed in terms of the processing time it took for one analysis. For the subset 1 analysed, the total processing time was 25.77 seconds in a PC with 2.40 GHz processor. The process that took the longest was the NFA computation at 24.22 seconds, followed by region growing at 1.37 seconds and finally gradient computation at 0.18 seconds. The processing time was also analysed for the 2 whole fields. The processing time for field 18 on UAV image of 20th August was 64.31 minutes. while that of field 23 on UAV image of 25th August was 48.12 minutes as seen in Table 5.1. Field 23 is smaller in size than field 18 by approximately 1160 Sq/m

The detection of crop rows using the UAV images was successful for the months of August for both fields, September for field 18 and October for field 23. Although not all the crop rows were detected, a majority of them were, compared to other dates. The detections were observed to deteriorate with each month in later stages of the crop growing season, especially for field 18. This could have been caused by more weeds growing taller between the rows making it hard to identify the crop row edges. It could have also been caused by the closing canopy of the crops hence, the space between the rows becoming unclear.

It was also observed that the detections were on one edge of the crop rows where the row formed a shadow. In some dates, the detections were on the right edges of the crop rows while in other dates it was

on the left edges. The result for UAV image of 25th August in field 23 resulted in rows being detected on the right-side edges of the rows while the UAV image of 27th October for the same field had crop rows detected on the left side. This could have been due to the images being capture off-nadir and also the effect of sun illumination angle during the capturing of images. The detection on one side only therefore, necessitated the approximation of the undetected edge of the crop row. This was done by calculating the orientation dominance of the detected lines and comparing them to the orientation dominance of the refence lines which was taken to represent that of the crop rows. The detected lines outside the range represented by crop rows were then discarded and the undetected edge was approximated at an offset distance of 0.5 m as discussed in Section 4.4. This proved to work well for the two fields where all the rows in each field were observed to have the same orientation.

It is possible to encounter a case where a field has rows with two main orientation dominance. For instance, a section of the field having crop rows with horizontal orientation and another section with vertical orientation. In such a case, one would then have to decide to either divide the field into two sections and apply LSD on each section separately, or apply LSD on the whole field and plot the orientation angle of the detected line segments in a histogram. The ranges in the histogram with the two highest peaks would then be regarded as the correctly detected crop rows.

Texture is an important property used for distinguishing features of interest in an image. The crop row detection was carried out using the UAV images with texture features extracted at different orientations, lag distances and window size as discussed in Section 4.1. The use of texture features did not help in improving the detection results.

6.1.2. Crop row detection on VHR satellite images

The detection using VHR satellite images in Mali was unsuccessful. For all the satellite images available throughout the entire growing season, there is not one imagery where the crop rows could be detected. As discussed in Section 5.5, the satellite images could have failed in detection due to the field characteristics in Mali. The crops are planted at very narrow spacing, hence, hard to identify the rows in satellite images at 2 m resolution. As the growing season progresses from planting to mid-season until harvesting, it was expected that the crop rows would be identified especially during mid-growing season when the crops have higher densities. According to the information provided by the STARS project, weeding was only carried out once in field 23, which was on 10th July 2014 but no more weeding was done after that. For field 18, no weeding was done during the entire growing season. This could result in weeds growing as tall as the crops, making it more for difficult to identify the crop rows at 2 m resolution.

The analysis of the WV-2 satellite image of Nigeria and also the work of Alemu (2016) on crop row detection in Nigeria, proved that the resolution of the satellite image could not be the reason for the failure in detection on its own. This is because the spatial and spectral characteristics of the WV-2 satellite imagery of Nigeria are the same as those of the WV-2 satellite imagery used in Mali.

6.2. Weeds analysis

The analysis of weeds was carried out after detection and masking of the detected crop rows from the UAV images. This was to ensure reduced confusion between crops and weeds in the fields. The SVM classifier requires tuning of parameters for each kernel, with each classification analysis (Lorena & De Carvalho, 2008). A grid search strategy was used for tuning of parameters where the algorithm was set to pick the same training samples for each iteration to give the best C value for Linear SVM and best C and γ

values for RBF SVM. The best parameter values obtained after the tuning process were used in classification of SVM maps

The weed detection results were affected by the initial detection of crop rows. There were some crop rows that were missed by the LSD algorithm and therefore, classified as weeds in the SVM classification. The missed detections on crop rows was mostly observed in late stages of the crop growing season. Looking at the weeds classification results of these dates, it was observed that the weed percentage cover was high, which was attributed to the classification of the missed crop rows as weeds.

Detection of weeds was also carried out on UAV images with texture features. This did not help in improving the classification results in weed detection, where the detection without texture features was observed to give more correct classification maps than with texture features.

The accuracy assessment using the overall accuracy and kappa coefficient values obtained did not prove to match up with some of the classification map results. This was observed in the detection of weeds before masking out of trees. The confusion between weed and tree classes was evident especially in subset 2 using the UAV image for the month of August. For the Linear SVM, most of the vegetation on the ground was classified as trees with very little classified as weeds while in RBF SVM for the same subset image, all pixels with vegetation were classified as vegetation. Even with these poor classification maps, the overall accuracy and kappa coefficient values were still high indicating that the result was acceptable yet it was not.

The overall weeds analysis from August to November showed an in increase in weeds cover in the farms every month. Although in some months the classification map results were poor due to the initial poor detection of crop rows, the increase in weeds every month could be true even though not by the values produced by the SVM algorithm. This is because of lack of weeding throughout the season as indicated earlier. The study by Njenga, (2016) of the same study area also showed increase in weeds in cotton fields every month and more weeds spread widely in November, towards the end of the crop season.

 Looking at the field reference data available, the result of weeds percentage cover for both fields agreed with it. The available field reference data was not adequate for the validation of the weeds as the analysis was done for the UAV images from the month of August to end the of November but, only field data for August and September was available. It was therefore not possible to validate the detected weeds for the other months.

7.   CONCLUSION AND RECOMMENDATIONS

7.1.   Conclusion

The main objective of this study was to develop a methodology for between-row weed detection in the fields using pattern and textural measures from UAV and VHR satellite images. The LSD algorithm was adopted for the detection of the crop rows. The SVM was then used to detect weeds between the rows. GLCM texture features were also extracted and used to assess the detection of the crop rows and weeds.

From the detection of crop rows using the LSD algorithm, it can be concluded that getting the optimal parameters is very important to ensure accurate detection results. The main internal parameters in the LSD algorithm are considered to be the scale, angle tolerance and epsilon. It is important to tune all the parameters including the gradient magnitude threshold and smallest region area threshold as not any parameter value used could give the expected results.

The efficiency of the LSD algorithm in terms of accuracy is input data dependent. The detections are not only affected by the spatial resolution of the imagery but also by the field characteristics. Not all images can have features being detected using this algorithm. Features in regions with low contrast that are homogenous in nature are hard to detect. This is the more reason why the detection on the VHR satellite images failed in this study. This could also be the reason for poor detection towards the end of the crop growing season on the UAV images. This is because the crops are dried up thus, low densities along the rows. There are also more weeds on the fields covering the crops, making the fields to appear more homogenous.

Texture features do not always improve detection and classification results. This could be due to the regions in the UAV images being homogeneous with low contrast. In this study, the texture features did not help improve the detection of crop rows and weeds.

An efficient algorithm should not only be accurate but also not time costly. In this study the LSD algorithm can be considered to be quite fast in terms of processing time. It worked well for the analysis with the longest time taken for an analysis done on the whole field being just above 1 hour. Some algorithms may take up to more than a day to produce a result and some would require high performance computer hardware for an analysis.

The optimal parameters for SVM classifier depend on the characteristics of the input data and also the training samples. It is therefore, important to tune parameters for each classification analysis. Using the search strategy set in the algorithm, the best parameters are selected and used in the classification of the maps. It can also be concluded from this study that, without successful detection of crop rows, the subsequent analysis of weeds is affected. This is because the crop rows that are missed to be detected in the LSD algorithm are classified as weeds in the weeds analysis.

The accuracy assessment of any analysis cannot be only verified using the various accuracy assessment methods in the algorithm. Visual verification is very important as some accuracy assessment results could show successful results which could be contrary to the actual results obtained. The reference data collected from the field is the most important in the verification of the results, otherwise it is hard to make conclusive observations.

7.2.   Recommendations

The quality of the input data has a large effect on the results for both crop row and weed detection. The UAV images used in the study are not of very high quality as the vegetation in the image appear to have the same colour. This means that the DN values for all types of vegetation in the image are similar. To curb this problem, colour correction could be performed on the UAV images to make them have more natural colour for various vegetation types on the ground. This may assist in improving analysis of weeds using the SVM classifier.

The manual masking of trees was observed to improve the classification results in the analysis of weeds. An automated way of masking of the trees on the UAV images could also be of great advantage to the successful weeds detection, especially when dealing with larger study areas.

More information on the field data would assist in better analysis of crop rows and weeds. Information on the row spacing and row widths for the different crop types at different growth stages would have assisted in determining the offset to be used when approximating the undetected edges of crop rows.

The reference data for weed cover provided was not adequate for analysis of weeds for the dates analysed. The reference data should be available, preferably for every month within the entire growing season to ensure more conclusive validation of the obtained results.

LIST OF REFERENCES

Ahmed, F., Al-Mamun, H. A., Bari, A. S. M. H., Hossain, E., & Kwan, P. (2012). Classification of crops and weeds from digital images: A support vector machine approach. *Crop Protection*, *40*, 98–104.

Akinlar, C., & Topal, C. (2011). EDLines: A real-time line segment detector with a false detection control. *Pattern Recognition Letters*, *32*(13), 1633–1642.

Alemu, M. M. (2016). *Automated farm field delineation and crop row detection from satellite images*. Retrieved from http://www.itc.nl/library/papers_2016/msc/gfm/alemu.pdf

Atkinson, J. T., Ismail, R., & Robertson, M. (2014). Mapping Bugweed (Solanum mauritianum) Infestations in Pinus patula Plantations Using Hyperspectral Imagery and Support Vector Machines. *IEEE Journal of Selected Topics in Applied Earth Observations and Remote Sensing*, *7*(1), 17–28.

Bekkari, A., Idbraim, S., Mammass, D., & El Yassa, M. (2011). Exploiting spectral and space information in classification of high resolution urban satellites images using Haralick features and SVM. *International Conference on Multimedia Computing and Systems -Proceedings*, 0–3.

Bergado, J. R. A. (2016). *A deep feature learning approach to urban scene classification*. Retrieved from http://www.itc.nl/library/papers_2016/msc/gfm/bergado.pdf

Bruzzone, L., & Persello, C. (2010). Approaches Based on Support Vector Machines To Classification of Remote Sensing Data. In *Handbook of Pattern Recognition and Computer Vision* (pp. 329–352). London, UK: ICP.

Burns, J. B., Hanson, A. R., & Riseman, E. M. (1986). Extracting Straight Lines. *IEEE Transactions on Pattern Analysis and Machine Intelligence*, *PAMI-8*(4), 425–455.

Calzadilla, A., Zhu, T., Rehdanz, K., Tol, R. S. J., & Ringler, C. (2013). Economywide impacts of climate change on agriculture in Sub-Saharan Africa. *Ecological Economics*, *93*, 150–165.

Clausi, D. A., & Ed Jernigan, M. (1998). A fast method to Determine Co--occurrence Texture Features. *IEEE Transactions on Geoscience and Remote Sensing*, *36*(1), 298–300.

Desolneux, A. (2016). When the a contrario approach becomes generative. *International Journal of Computer Vision*, *116*(1), 46–65.

Desolneux, A., Moisan, L., & Morel, J.-M. (2008). *From Gestalt Theory to Image Analysis*: *A probabilistic Approach*. (Vol. 34). Springer: New York.

Desolneux, A., Moisan, L., & Morel, J. M. (2000). Meaningful alignments. *International Journal of Computer Vision*, *40*(1), 7–23.

Desolneux, A., Moisan, L., & Morel, J. M. (2003). Maximal meaningful events and applications to image analysis. *Annals of Statistics*, *31*(6), 1822–1851.

Duda, R. O., & Hart, P. E. (1972). Use of the Hough transform to detect lines and cures in pictures. *Communications of the Association Computing Machinery*, *15*(1), 11–15.

Etemadi, A. (1992). Robust segmentation of edge data. *Int. Conf. on Image Processing and Its Applications*, 311–314.

FAO. (2015). Achieving Zero Hunger: The Critical Role of Investments in Social Protection and Agriculture. Retrieved June 2, 2016, from http://www.fao.org/documents/card/en/c/91014696-3723-4df5-b729-2b4e55b22e8f/

Fernandes, L. A. F., & Oliveira, M. M. (2008). Real-time line detection through an improved Hough transform voting scheme. *Pattern Recognition*, *41*(1), 299–314.

Grompone von Gioi, R. (2014). *A Contrario Line Segment Detection*. New York: Springer.

Grompone Von Gioi, R., Jakubowicz, J., Morel, J.-M., & Randall, G. (2012). LSD: a Line Segment Detector. *Image Processing On Line*, *2*, 35–55.

Haralick, R. M., Dinstein, I., & Shanmugam, K. (1973). Textural features for image classification. *Transactions on Systems, Man, and Cybernetics, 3(6)*.

Hough, P. V. C. (1962). Method and means for recognizing complex patterns. *US Patent 3,069,654*.

Kiryati, N., Eldar, Y., & Bruckstein, A. M. (1991). A probabilistic hough transform. *Pattern Recognition*, *24*(4), 303–316.

Kuntagod, N., Paul, S., Kumaresan, S., Ganti, S., & Yala, G. (2016). Last-mile wireless connected crop solution for smallholder farmers: Profitably connecting all the major players in the agriculture ecosystem in rural areas. *IEEE Asia Pacific Conference on Wireless and Mobile*, 130–135.

López-Granados, F., Torres-Sánchez, J., Serrano-Pérez, A., de Castro, A. I., Mesas-Carrascosa, F.-J., & Peña, J.-M. (2016). Early season weed mapping in sunflower using UAV technology: Variability of herbicide treatment maps against weed thresholds. *Precision Agriculture*, *17*(2), 183–199.

Lorena, A. C., & De Carvalho, A. C. P. L. F. (2008). Evolutionary tuning of SVM parameter values in multiclass problems. *Neurocomputing, 71*(16–18), 3326–3334.

Malegori, C., Franzetti, L., Guidetti, R., Casiraghi, E., & Rossi, R. (2016). GLCM, an image analysis technique for early detection of biofilm. *Journal of Food Engineering, 185*, 48–55.

Nations Encyclopedia. (2015). Agriculture - Mali - area, crops, farming, infrastructure. Retrieved January 30, 2017, from http://www.nationsencyclopedia.com/Africa/Mali-AGRICULTURE.html

Ni, J., Khan, Z., Wang, S., Wang, K., & Haider, S. K. (2016). Automatic Detection and Counting of Circular Shaped Overlapped Objects Using Circular Hough Transform and Contour Detection. *12th World Congress on Intelligent Control and Automation (WCICA)*, (Kylx15 0496), 2902–2906.

Njenga, G. W. (2016). *Multiple Endmember Spectral Mixture Analysis (MESMA) on multi-temporal VHR images for weed detection in smallholder farms* . University of Twente Faculty of Geo-Information and Earth Observation (ITC). Retrieved from http://www.itc.nl/library/papers_2016/msc/gfm/njenga.pdf

Otsuka, K., & Kalirajan, K. (2008). *Agriculture in Developing Countries : Technology Issues*. New Delhi: SAGE India.

Pierce, F. J., & Clay, D. (2007). *GIS applications in agriculture*. Baton Rouge: CRC Press.

Richards, J. A. (2013). *Remote Sensing Digital Image Analysis. Methods.* (5th ed.) Berlin, Heidelberg: Springer

Rougier, S., Puissant, A., Stumpf, A., & Lachiche, N. (2016). Comparison of sampling strategies for object-based classification of urban vegetation from Very High Resolution satellite images. *International Journal of Applied Earth Observation and Geoinformation*, *51*, 60–73.

Sardana, V., Mahajan, G., Jabran, K., & Chauhan, B. S. (2016). Role of competition in managing weeds: An introduction to the special issue. *Crop Protection*, 1–7.

Sidiropoulou Velidou, D., Tolpekin, V. A., Stein, A., & Woldai, T. (2015). Use of Gestalt Theory and Random Sets for Automatic Detection of Linear Geological Features. *Mathematical Geosciences*, *47*(3),

Song, L., Smola, A., Gretton, A., Bedo, J., & Borgwardt, K. (2012). Feature selection via dependence maximization. *Journal of Machine Learning Research*, *13*, 1393–1434.

STARS, & ICRISAT. (2014). DBSTARS-Mali- Minventaire picture. *STARS Project and ICRISAT*.

STARS, & ICRISAT. (2015). STARS-ISABELA-Mali - Metadata documentation. Field measurements campaign 2014 in Mali.

Teutsch, M. (2014). Moving Object Detection and Segmentation for Remote Aerial Video Surveillance - Google Books. Retrieved February 8, 2017, from https://books.google.nl/books?id=PQGGBwAAQBAJ&printsec=frontcover&hl=nl&source=gbs_ge_summary_r&cad=0#v=onepage&q&f=false

Ursani, A. A., Kpalma, K., Lelong, C. C. D., & Ronsin, J. (2012). Fusion of textural and spectral information for tree crop and other agricultural cover mapping with very-high resolution satellite images. *IEEE Journal of Selected Topics in Applied Earth Observations and Remote Sensing*, *5*(1), 225–235.

Vintrou, E., Houles, M., Lo Seen, D., Baron, C., Feau, C., Laine, G., & Bégué, A. (2009). Mapping cultivated area in West Africa using MODIS imagery and agroecological stratification. *International Geoscience and Remote Sensing Symposium (IGARSS)*, *5*, 393–396.

Xu, L., Oja, E., & Kultanen, P. (1990). A new curve detection method: Randomized Hough transform (RHT). *Pattern Recognition Letters*, *11*(5), 331–338.

Zongjian. (2008). Uav for Mapping — Low Altitude Photogrammetric Survey. *The International Archives of the Photogrammetry, Remote Sensing and Spatial Information Sciences*, *XXXVII*(Part B1), 1183–1186. Retrieved from http://citeseerx.ist.psu.edu/viewdoc/download?doi=10.1.1.150.9698&rep=rep1&type=pdf

Appendix
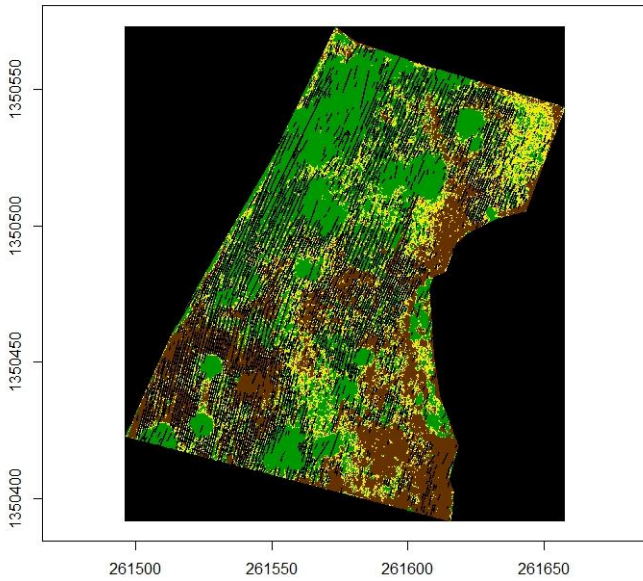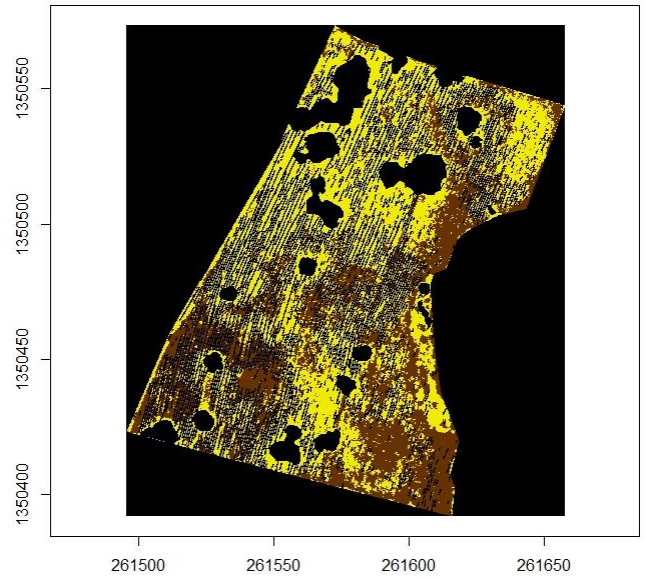
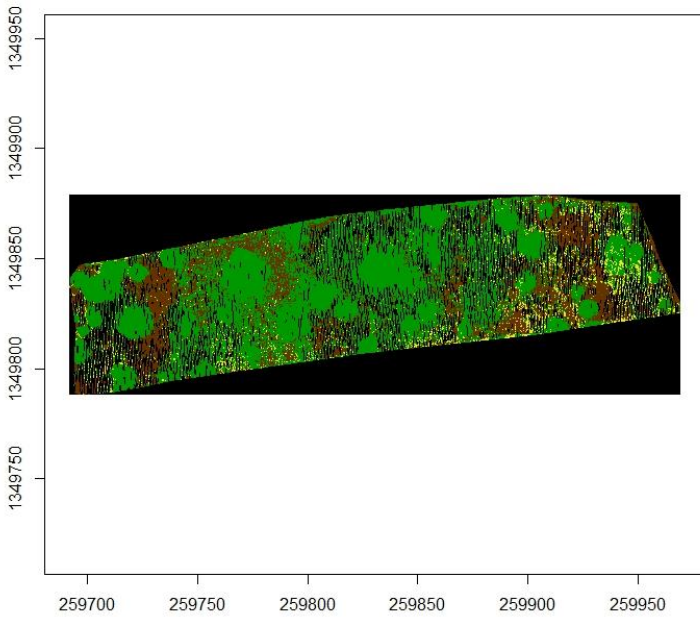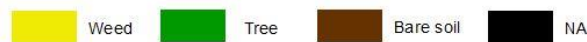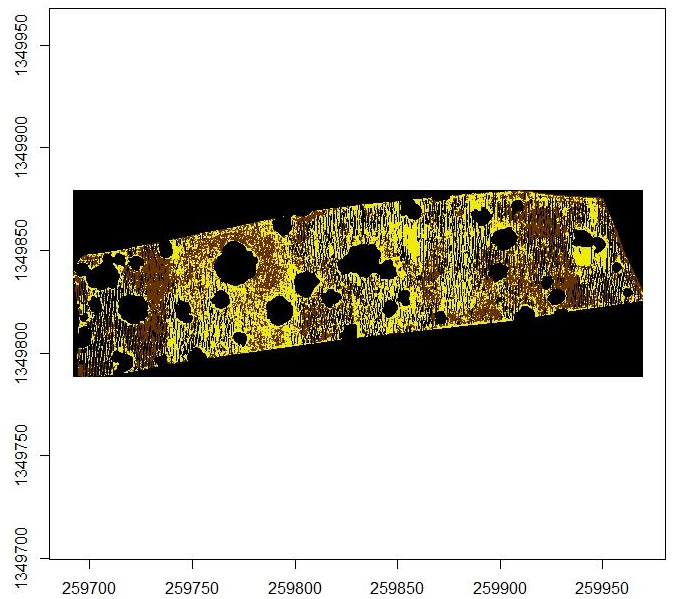Result of RBF SVM for field 23 before unmasking of trees and after tree masking on the UAV image of 25th August 2014

Result of RBF SVM for field 18 before unmasking of trees and after tree masking on the UAV image of 11th September 2014